Simulation and Modelling of Interference and Shadowing in LMCS

By

J.C. Bronson, B.Eng., P.Eng.

A thesis submitted to the

Faculty of Graduate Studies and Research

In partial fulfillment of

The requirements for the degree of

Master of Engineering

Ottawa-Carleton Institute for Electrical and Computer Engineering

Department of Systems and Computer Engineering

Carleton University

Ottawa, Ontario

May, 2000

ABSTRACT

Recently, efforts are being made to provide broadband services to fixed residential and commercial subscribers through wireless cellular networks called Local Multipoint Communication Service (LMCS). In order to compete with established wireline services, the problem of providing reasonably comparable coverage must be overcome. Generally, there is a lack of specific propagation information at EHF frequencies. This radio propagation data is required for systems to be designed that can successfully adapt to local propagation environments. The object of this research is to gather field measurements and apply the propagation information to simulation and modelling in order to predict interference and shadowing impairments likely to be experienced in an LMCS environment.

The field measurements at 29.5 GHz in an urban environment observed a pathloss exponent of 4.01 for NLOS propagation paths. The standard deviation of shadowing experienced was 13.89 dB and was thus consistent with other research.

Simulation shows that the interference expected in a LMCS can significantly impact the performance. A simplified interference model shows that the propagation exponent and standard deviation of shadowing considerably affect outage probability. Antenna characteristics such as beam width, gain ratio, and beam pattern were also evaluated for their effects on outage. Further, sectoring proved to dramatically reduce the outage experienced at the base station. The distribution of interference powers at a base station is shown to have a log-normal distribution using the Kolmogorov-Smirnov Test.

ACKNOWLEDGEMENTS

My gratitude goes to Professor David Falconer, my supervisor, for his instruction, guidance, patience, and encouragement throughout the course of this research. His efforts contributed directly to the success of this thesis, and to my enjoyment of it.

Dr. Robert Bultitude offered me the benefit of his experience on more than one occasion. I am grateful for his assistance during the field measurements portion of this research.

My thanks also go to Mr. Bob Hahn, firstly, for constructing the radio equipment I used for the fieldwork, and secondly, for graciously providing access to the technical specifications.

John Sydor and Alain Dugais assisted my field work by giving me the benefit of their previous work in the Glebe and facilitating my access to the roof of Glebe High School.

My appreciation goes to the following graduate students for the beneficial discussions and consultations: Jean-Paul DeCruyenaere, and Sébastien Roy. On several occasions, they offered their time and energy during busy periods. Thanks!

Special thanks to Nausheen Naz for instructing me on the operation of the CW equipment and especially for the use of her LabView program used to control the CW receiver.

Finally, I am most grateful for the continual support and encouragement of my close friends and family. This work would not have been completed if they had let me complain or procrastinate.

TABLE OF CONTENTS

LIST OF FIGURES

LIST OF ACRONYMS

ACI	Adjacent Channel Interference
BS	Base Station
CCI	Cochannel Interference
DAQ	Data Acquisition
EHF	Extremely High Frequency
EIRP	Effective Isotropic Radiated Power
FSPL	Free Space Path Loss
IF	Intermediate Frequency
IFBW	Intermediate Frequency Bandwidth
LMCS	Local Multipoint Communication Service
LMDS	Local Multipoint Distribution Service
LOS	Line-of-sight
NF	Noise Floor
NLOS	Non-Line-of-sight
PCMCIA	Personal Computer Memory Card International Standard
QPSK	Quadrature Phase Shift Keying
RSL	Received Signal Level
SINR	Signal to Interference and Noise Ratio
SIR	Signal to Interference Ratio
SNR	Signal to Noise Ratio
T-R	Transmitter to Receiver

Chapter One

INTRODUCTION

1.1 Thesis Objectives

Recently, much effort is being brought to bear to provide broadband services to fixed residential and commercial subscribers through wireless cellular networks. These networks are collectively termed, Local Multipoint Communication Services (LMCS) in Canada, or Local Multipoint Distribution Services (LMDS) in the United States. Industry Canada has opened up six 500 MHz blocks of bandwidth in the 26-28 GHz range for LMCS providers [1]. However, the propagation environment at EHF frequencies is not well understood and radio waves of these frequencies suffer several propagation impediments making reliable coverage difficult to attain.

LMCS success is dependent on the technology costs of the EHF radio equipment and the provision of quality of service guarantees [2]. The propagation problems at EHF frequencies must be transparent to the end-user and, in order for LMCS providers to compete with established wireline (cable) services, the problem of providing reasonably comparable coverage must be overcome. Generally, there is a lack of specific information regarding propagation at EHF frequencies. This radio propagation data is required in order for systems to be designed that can adapt to local propagation environments in the most economical fashion.

The object of this research is to gather field measurements to evaluate the LMCS radio channel in a non-line-of-sight (NLOS) environment. The observed propagation parameters will be used in a computer simulation to model the predicted path loss in a LMCS network. The intent of the simulation and modelling is to evaluate interference likely to be experienced in an LMCS network.

The simulation will investigate the effect on total interference of several parameters of LMCS design. These parameters are: propagation exponent, standard deviation of log-normal shadowing, antenna design (beam width, gain ratio), sectoring, and base station diversity.

1.2 Thesis Organization

This thesis is organized into six chapters. Chapter 1 is the introduction and describes the objectives, organization, and contributions of this thesis. In Chapter 2, a description of LMCS and factors affecting performance are presented including reference to the published research in this area. In addition, the theoretical background of the interference model is presented. A review of communication theory relevant to this work is contained in Chapter 3.

In support of this research, field measurements were taken in an urban area in Ottawa. Chapter 4 presents the measurement plan, equipment, analysis and results. In addition, the results of these measurements are compared with measurements taken by other sources at the same frequency.

A computer simulation of a LMCS network was developed to predict the level of interference and to investigate the effect of various parameters on interference received by the base station. The model parameters, simulation results, goodness of fit tests, and a discussion of what this simulation reveals is found in Chapter 5.

Finally, the conclusion and recommendations for future research are found in Chapter 6.

1.3 Thesis Contributions

The major contribution of this thesis is to identify the interference that can be expected at the base station of a cell in a LMCS network. Propagation measurements are used to produce a more statistically significant simulation of the interference in a LMCS network.

The fieldwork of this thesis contributes more propagation measurements to the limited body of data at this frequency. The observed path loss exponent along with the standard deviation of log-normal shadowing are found to be consistent with previously reported results.

A simplified interference model introduced in Section 5.1.2 is used to construct a simulation of a LMCS network. Simulation results reveal the limitations on system performance that interference in a LMCS system imposes. A high propagation exponent is demonstrated to reduce the outage probability by attenuating interfering signal levels. Antenna design and sectoring is shown to affect LMCS performance by reducing

interference levels. Further, simulated base station diversity has been shown to reduce the outage probability experienced at the base station and is an important component of LMCS design.

The distribution of interference powers at a base station is shown to have a log-normal distribution using the Kolmogorov-Smirnov Test on a logarithmic scale at a significance level of 0.1.

Chapter Two

LMCS SYSTEM

This chapter describes the Local Multipoint Communication System (LMCS) and its main characteristics. Background information is provided concerning the conception, development, configuration, frequency allocation, and antenna design of LMCS systems. The advantages and disadvantages of an LMCS system are discussed. Next, a review of the research concerning the primary factors affecting LMCS performance is presented. Reference is made concerning how each factor is investigated in this work. Finally, the methods used to model log-normal random variables are described with particular note of the method used in this work.

2.1 LMCS System

In the past, there was minimal technology development at high frequencies. Recently, the increasing ability to produce radio equipment that can operate at higher and higher frequencies yet retaining low costs has raised the concept of providing fixed broadband wireless services to commercial and residential subscribers. New systems are being developed for the microwave and millimetre wave frequencies [3]. Indeed, frequency bands in the area of 27.5-29.25 GHz have been opened for licensing applications in Canada [1]. In the United States, this system is called Local Multipoint

Distribution Service (LMDS) whereas Canada has adopted the LMCS name. Industry Canada has authorized a frequency band in the 28 GHz range for LMCS use.

LMCS will provide terrestrial bi-directional wireless broadband services for multimedia applications such as broadband Internet, video conferencing, video-on-demand, telephony, and data access services. LMCS is designed as a cellular system with overlapping cells usually with a radius of one to five kilometres.

The main advantage of the LMCS system is that a system can be deployed rapidly and easily with lower infrastructure cost compared with traditional cable-based broadband services [4]. For example, setting aside the base station and their wire-based interconnections, to set up a new LMCS system, a provider need only mount a small antenna on or near the roof of a potential subscriber's home. This rapid, low-cost deployment may prove particularly useful in developing areas or in northern regions where a cable infrastructure is not already available.

Another advantage is the elimination of the dependence on the local loop [2]. This will provide formidable competition to the cable and telephony based providers who have, until now, relied on the fact that their infrastructure is available and readily upgradeable.

Of course, LMCS, like all other outdoor wireless cellular systems, is subject to co-channel interference (CCI), which is its primary disadvantage. CCI can become significant enough to reduce serviceable coverage. Compared with cable-based broadband services, which, for all practical purposes, enjoy 100% coverage, broadband

wireless offers a viable alternative, but only to a reduced number of potential subscribers due to the challenging propagation environment. So, it is incumbent on providers to maximize coverage yet retain low cost.

Coverage issues are a great challenge for providers due to the propagation environment that may require line-of-sight (LOS) propagation paths since millimetre waves do not easily penetrate trees or buildings. However, LOS paths are not always readily available in a residential community. Further, movement of foliage and traffic has been shown to cause detrimental fading of the signal envelope of communication links at these high frequencies [5]. So, use of NLOS propagation paths is necessary to realize the maximum possible coverage in urban and suburban areas.

Many LMCS system designs rely on assumed radio propagation information. Modelling wave propagation has only recently received attention by researchers at these EHF frequencies [6]. As more companies develop their enabling technologies, more relevant radio propagation data will become available. The object of this work is to use information derived from field measurements to construct an accurate interference model.

2.1.1 Basic Configuration

A typical LMCS system is arranged in a cellular network much like mobile phone networks. Each cell is approximately 1-5 km in radius and are over-lapped. The base stations in each cell are interconnected through a wireline network. The basic configuration of a LMCS network is shown in Figure 2.1.

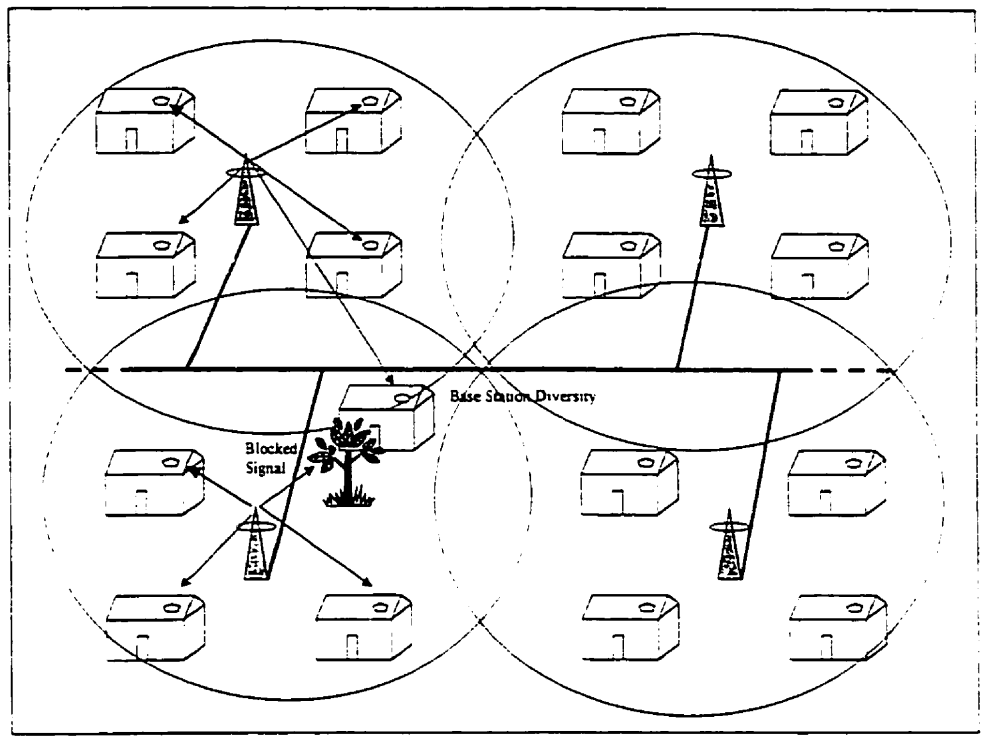

Figure 2.1 LMCS Configuration

In some cases, if a direct LOS path cannot be provided, use of repeaters will allow access to subscribers, who would not normally have sufficient signal-to-interference plus noise ratio (SINR) for adequate service.

Cells are overlapped to provide maximum attainable coverage. If a subscriber cannot establish an adequate link to the base station nearest its location, it may communicate with an adjacent base station should a link be available. In Figure 2.1, a large tree blocks a link between a subscriber and its closest base station so that a link with an adjacent base station is used. This is termed base station diversity and is incorporated into the simulation presented in Chapter 5. It is also possible for multiple links to be

combined to yield an adequate SINR, but that more sophisticated technique is not explored in this work.

2.1.2 Frequency Allocation

Industry Canada has recognized the emerging technology and potential for broadband services. Bands in the 27.35 to 28.35 GHz have been opened to licensing applications [1]. There are currently three licensed LMCS carriers in Canada. Cellular Vision Canada Ltd., MaxLink Communications Inc., and RegionalVision Inc. were awarded licences in May 1996 [7]. MaxLink holds licences for every major urban centre in Canada. New licences for the 24 and 38 GHz bands will soon be auctioned [8].

2.1.3 Antenna Design

The antennas affixed to the subscriber's home are highly directive so as to reduce the co-channel interference. The base station is divided into sectors covering the full 360°, for example, a three-sector hub would have each of its antennas covering 120° whereas a four-sector hub would have each antenna covering only 90°.

Recommended LMCS antenna specifications can be found on the website of the IEEE 802.16 Working Group on Broadband Wireless Access Standards [9]. The purpose of the Coexistence Task Group (802.16.2) is to minimize interference so that maximum system performance and service quality can be realized. Technical antenna specifications that will achieve this goal are currently being researched.

2.2 Factors Affecting System Performance

The performance of a LMCS system is affected by many factors such as propagation environment, sectoring, antenna design, and power control. These factors are described in this section with reference to relevant research. Reference is made as to how each factor is investigated in this work.

2.2.1 Propagation Environment

The outdoor propagation environment is subject to many impediments, and this is particularly true at the frequencies of interest for LMCS. The most significant propagation issues are path loss, signal attenuation by rain, foliage, and buildings, signal depolarization, multipath, interference, and shadowing [10].

Millimetre waves exhibit quasi-optical behaviour and are significantly attenuated by obstructions such as trees and buildings [11]. Usually, no signals can be detected through steel reinforced concrete or brick buildings [12]. With the LMCS subscriber antennas located on or near the roof, the radio path is frequently expected to be below the treetops, especially in well-established communities containing mature trees. Thus, there will be a significantly high probability of non-LOS paths in any deployment plan for a typical urban or suburban area.

Research by Seidel and Arnold [13] found that building blockage would significantly limit coverage of any area. Antenna height was found to play an important role as the signal was often lost once the receiver antenna was lowered below roofline. As well, specular reflections were found in many receiver locations but were not

concluded to have a significant effect on coverage. Indeed, the maximum signal level is almost always found to be in the direction of the transmitter.

Another study of the LMCS radio channel by Papazian, et al. [10] predicts coverage from attenuation measurements taken in urban and suburban areas. Signal attenuation was found to be the most significant propagation impairment, especially when the tree canopy extended above the roof height. Further, the primary mode of propagation was thought to be diffraction.

Chua, et al. found propagation measurements at 27.4 GHz followed the free space loss curve with excess losses ranging from 24-60 dB [4].

Naz reports that trees can cause significant attenuation and signal variability due to movement by wind [5]. Single tree attenuation is on the order of 30 dB [14]. Fade rates were found to be greater for foliage movement than for vehicular movement. Indeed, with LMCS signals at roof level, there is a greater chance that trees will cause blockage than will vehicles on the road.

The goal of the fieldwork in this research is to obtain a series of measurements, which will yield a greater understanding of the LMCS radio channel. Specifically, the propagation exponent and the degree of shadowing (as measured by standard deviation of log-normal shadowing) is sought. These measured parameters will be directly used to construct a model of a LMCS network.

2.2.2 Sectoring

A typical method used in cellular networks to combat co-channel interference (CCI), is to divide a cell into sectors. A base station omni-directional antenna can be replaced with several antennas each of which only covers a portion of the 360° cell [15]. For example, each antenna in a base station with four sectors would cover 90°.

The amount of sectoring used directly affects the degree to which CCI is reduced. However, there is a corresponding loss of traffic due to trunking inefficiency and increased operating complexity [15].

The simulation presented in Chapter 5 will compare the interference levels exhibited in an undivided cellular network with that found in a network in which sectoring has been applied. Three, four, six, and 12 sector models will be constructed and evaluated by comparing their outage probabilities with that of an omni-directional system (no sectoring).

2.2.3 Antenna Design

Due to increased congestion of the frequency spectrum and the increased potential for interference, LCMS design typically calls for highly directive subscriber antennas with high gain and good polarization. A directive antenna will reduce CCI [14].

Simulation will be conducted to determine the effect of both subscriber and base station antenna beam width along with their respective gain ratios. Antenna gain ratio is the ratio between the maximum gain of the main beam to the maximum gain of the

secondary beam. In the simulation, the antenna beam patterns will be modelled as two-valued so that the antenna gain ratio is simply the difference between them in dBs.

Simulation will also compare expected interference levels from ideal antenna design with that of a realistic antenna design. This is done by Newson and Health [16] for a CDMA channel. They found a reduction of simulated network capacity when realistic antenna patterns were used.

2.2.4 Power Control

In order to reduce the interference present in a cellular network, control is often exercised over the power at which transmitters operate. This positive control ensures that only the minimum power required for an adequate communication link is used, which results in an overall drop in system interference and better SINR at the base station receiver. The simulation will model power control to ensure that each subscriber transmits at a power that compensates for path loss and provides a fixed receive power at the receiver.

Since LMCS will employ this performance enhancing technique, the subscribers in the forthcoming simulation will have a simulated transmitter power that is a fixed value at the receiving base station. That is, the path loss will be calculated between the subscriber and its base station, then the subscriber will be given an output power that is the fixed value plus the simulated path loss. This way, each base station will receive a fixed signal level from its subscribers, but the interference that occurs will depend on distance, path losses, and antenna gains.

Figure 2.2 illustrates how the simulation will model power control. The transmit power of the subscriber is set to 130 dBm such that the fixed value of 30 dBm will be received by the base station with the lowest path loss (100 dB). Note that antenna gains and directivity have been neglected in this example.

It is important to note that the transmit and receive powers shown in Figure 2.2 are for illustration purposes only. The actual power control correction at the transmitter would be proportional to the actual path loss, not equal to it so that the transmit power is kept reasonable (for example, between 20 dBm and 0 dBW).

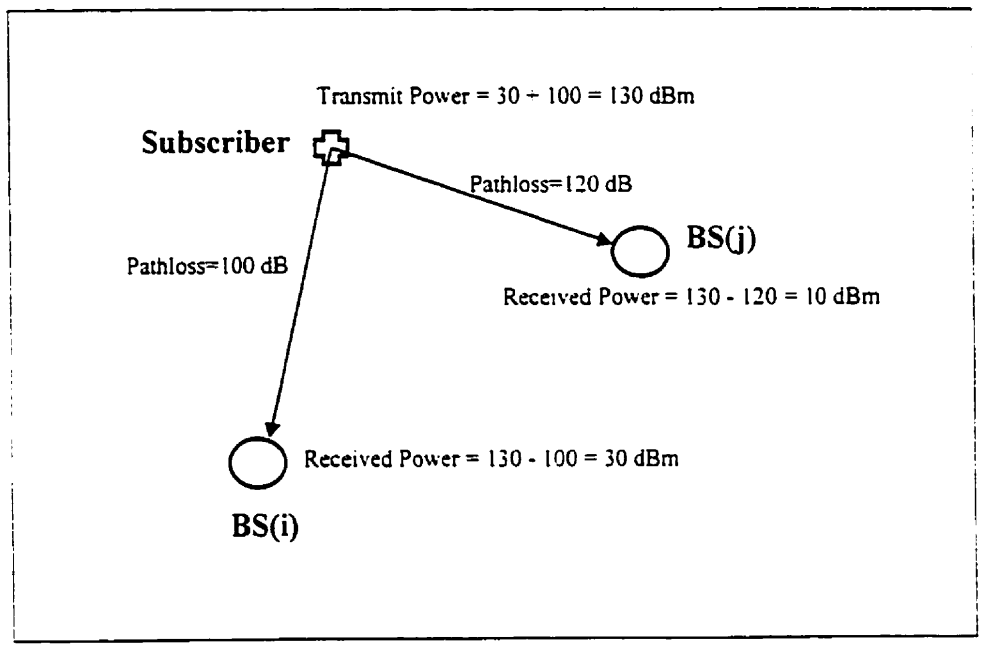

Figure 2.2 Power Control

Imperfect power control has been found to have two effects [16]. First, power control errors will change the statistics of the interference for all users. Secondly, the required signal will undergo significant variation when imperfect power control is

experienced. The second effect has a more detrimental effect on system performance. Interleaving and coding are techniques that can be used to counter the detrimental effects of imperfect power control.

2.3 Modelling of Interference in LMCS

This section presents an overview of the theoretical considerations of modelling interference in a LMCS network. In the forthcoming simulation, log-normal shadowing will be modelled as a Gaussian random variable (in units of dB) which adds to the transmitted power of an interferer. The multiple log-normal interfering signals are added for a total interference value. Thus, the following is a review of the relevant research in the area of combining multiple log-normal random variables and provides a theoretical basis for the modelling technique used in Chapter 5.

Since the shadowing random variable can be either positive or negative, the resulting receive power at the base station may be greater or less than that which just undergoes pathloss. Of course, the mean received signal will be lower in a shadowing environment than one free of shadowing. Log-normal shadowing will usually occur reciprocally in both the uplink and downlink channels [13].

Computation of the distribution of a sum of multiple log-normal random variables occurs often in communications work. Despite much work in this area, a closed form solution has not been discovered [18-20]. Thus, a way to model the sum of multiple correlated log-normal random variables has been the subject of much research.

Beaulieau, et al, compare several methods of predicting the distribution of a sum of multiple log-normal random variables and found that a relatively simpler method by Wilkinson yields a reliably more accurate result than the more popular method by Schwartz and Yeh [21].

An approximate technique, described by Schwartz and Yeh in [22], is used for simple and accurate calculations of co-channel interference caused by log-normal shadowing in mobile telephony. They also show a large sensitivity to propagation parameters in [21].

Linnartz offers an alternative method of calculating the outage probability without making approximations to the probability distribution of the interference power accumulated from several log-normal signals [23]. This method proved to be faster in terms of numerical analysis and no restriction is imposed on the standard deviation of shadowing as with the previous methods.

The above methods assume that the interfering signals are uncorrelated. Abu-Dayya and Beaulieau have conducted work with the opposite assumption [24]. They stipulate that the same obstacle near the receiver may shadow multiple interfering signals. Three methods are evaluated and determined to render similar results. As well, Safak found accurate results for correlated interfering signals when compared with Monte-Carlo simulation [21].

Newson and Heath provide some insight into calculation of interference in a cellular network [16]. Realistic antenna patterns and power control errors are

investigated for their effects on the capacity of a CDMA system. The geometry used in the forthcoming simulation is similar to that used in Newson and Heath's article.

Zorzi offers insight into the calculation of interference statistics [25]. The analytical framework provided includes distance path-loss, log-normal shadowing, best cell site selection, and power control. A similar method is adapted in the model presented in Chapter 5.

Chapter Three

RELEVANT COMMUNICATION THEORY

This chapter contains the relevant communication theory on which this work is primarily based. Path loss, interference, log-normal shadowing, diversity, and power control are discussed in detail with reference to how these factors are accounted for in the field measurements and in the model and simulation.

3.1 Path Loss

Wireless communication relies on electromagnetic waves to send a signal from origin to destination. The behaviour of EM waves can generally be grouped into reflection, diffraction, and scattering [14, 15]. There are many models that have been developed in an effort to predict the average signal strength at the receiver for a given transmitter-to-receiver (T-R) distance. Propagation models can generally be classified as either *large-scale* model or *small-scale (fading)* [26]. Large-scale models predict the average signal strength over large periods of time or over large propagation distances whereas small-scale models are concerned with the signal strength over short periods of time or over small propagation distances. This work is primarily concerned with large-scale propagation modelling.

3.1.1 Free Space Path Loss

The outdoor propagation environment endures path loss from several sources. Free space imposes a path loss according to the standard equation [15, 27]:

$$P_r = P_t \cdot G_t \cdot G_r \cdot (\frac{\lambda}{4\pi d})^2 \qquad (3.1)$$

where: P_r, P_t are the received signal power and the transmitted signal power, respectively.

G_t, G_r are the transmitter and receiver antenna gains, respectively,

λ is the wavelength of the signal, and

d is the distance from the transmitter to the receiver (T-R distance).

Note the second-power distance dependence. This is considered the ideal case, or the minimum path loss that will be experienced. Of course, actual propagation scenarios will experience significantly greater path loss due to impediments of the local environment. It should be noted that propagation exponents of less than 2 have been observed in situations where the radio waves are guided. For example, signal energy can be channelled by a street yielding less path loss than that predicted by the free space model.

In the proposed LMCS scenarios, the frequency of use is in the range of 28 GHz, providing a wavelength of 1 cm. Unfortunately, this high frequency, although providing the necessary bandwidth, endures much attenuation from trees, buildings and even local weather. Objects that are approximately 1 cm in size, such as rain drops or leaves, can significantly disrupt radio waves of 28 GHz. In addition, street orientation has been found to channel the signal energy such that the strongest signal paths are not from directions of direct paths diffracted over the nearest building, but are from directions parallel to the streets [27].

3.1.2 Ground Reflection Path Loss

The free space path loss model accounts for the situation where there is only a direct path between the transmitter and the receiver. Since a direct path is unlikely in real propagation environments, a new model, which accounts for a variety of propagation paths is desired. When one considers the situation where the T-R distance is much greater than the height of the transmitter, neglecting the curvature of the earth's surface, then a modified path loss equation has been found to apply [4, 28]:

$$P_r = P_t \cdot G_t \cdot G_r \cdot (\frac{h_t h_r}{d^2})^2 \qquad (3.2)$$

where: h_t, h_r are the heights of the transmitter and receiver, respectively. Here, a fourth-power distance dependence is present. Thus, a propagation exponent of approximately 4 or greater is expected from the field measurements.

3.2 Interference

In cellular communications systems, there are two types of interference that are of concern: co-channel interference and adjacent channel interference. Both directly affect the performance of a wireless communications network by reducing the signal to interference plus noise ratio (SINR) at both the subscriber and base station.

3.2.1 Co-channel Interference

Co-channel interference (CCI) occurs when two or more transmitters are assigned the same frequency. CCI must occur in any cellular network due to the necessity of

frequency reuse; the radio spectrum is finite and a limited set of frequencies is available to any one system. Thus, a reduction in the degree of frequency reuse will subsequently reduce the amount of CCI that occurs in a network. However, reducing the frequency reuse is often challenging in a congested radio spectrum.

The signal to interference ratio at the base station in a LMCS network can be expressed as [14]:

$$\frac{S}{I} = \frac{S}{\sum_{k=1}^{N} I_k} \tag{3.3}$$

Where S is the desired signal power.

I_k is the interference power contributed by interfering subscriber k, and

N is the total number of interfering signals.

The total number of interferers depends on the cellular geometry and the frequency reuse pattern.

Co-channel interference is directly calculated in the simulation presented in Chapter 5. The total interference power contributed by a single subscriber is calculated and used to evaluate the interference considerations of a LMCS system. Factors affecting the levels of interference at the base station are investigated. Propagation parameters observed in the field measurements will be applied to yield a more accurate simulation of interference in a LMCS network.

3.2.2 Adjacent Channel Interference

Interference from neighbouring channels is called adjacent channel interference (ACI). Neighbouring channels will only cause interference if the receiver does not perfectly filter incoming signals. Therefore, proper filtering and maximizing the frequency separation of adjacent channels can reduce ACI.

Typically, LMCS reuses the whole frequency spectrum and thus CCI will be the dominant type of interference encountered in a LMCS system. Therefore, only CCI is considered in this work.

3.3 Log-Normal Shadowing

Another significant factor regarding propagation, which must be accounted for in any model, is that of shadowing. Although two different locations may have the same T-R distance, they may endure significantly different path losses. The determining factor is the propagation path(s) taken and the degree of environmental clutter along each path. Thus, actually measured signals may greatly differ from that predicted by Equation 3.1 or 3.2. Measurements have reliably shown that for a given T-R distance, the path loss is generally random with a log-normal distribution [27]. That is, the distribution of path losses measured in dBs is normal (Gaussian).

The following equations from [4] illustrate this point:

$$PathLoss = \overline{PL}(d) + \chi_\sigma \qquad (dB) \tag{3.4}$$

$$PathLoss = \overline{PL}(d_o) + 10n\log(\frac{d}{d_o}) + \chi_\sigma \tag{3.5}$$

where: $\overline{PL}(d)$ is the average path loss at T-R distance d,

χ_σ is a zero-mean Gaussian random variable with standard deviation σ (both in dB) which represents the shadowing component of the propagation,

n is the path loss exponent, and

d_o is a reference distance at which actual propagation measurements have been taken [29].

The path loss (or propagation) exponent is a measure of the rate at which path loss increases with distance. The reference distance, path loss exponent, and the standard deviation of the Gaussian distribution collectively describe the statistics of the propagation environment.

A shift in reference distance has been shown to affect the mean decay power [29]. So, a reference distance appropriate to the local propagation situation must be chosen when using Equations 3.4 or 3.5 as it will alter the predicted pathloss.

The standard deviation of the shadowing component – the degree of shadowing – is usually found to be a value from 4 to 10 dB [30, 31]. In this work, the actually observed value from the field measurements is used in the simulations.

Log-normal shadowing occurs when the measured signal level in dB units at a particular T-R separation follow a Gaussian distribution according to:

$$x = 10\log r \tag{3.6}$$

$$P(x) = \frac{1}{\sigma\sqrt{2\pi}}\exp\left(\frac{-(x-\mu)^2}{2\sigma^2}\right) \tag{3.7}$$

where: P(x) is the probability density function of a Gaussian distribution,

r is a log-normal random variable,

μ is the mean of the log-normal random variable, and

σ is the standard deviation of the log-normal random variable.

In a cellular network, a receiver will likely encounter multiple interfering signals each of which will endure log-normal shadowing. Thus, this interference is usually modelled itself as a log-normal random variable and there are various methods of combining the component means and standard deviations to form the model distribution [18].

3.4 Diversity

Diversity refers to a situation where multiple methods of transmitting a signal are available to a given communication. Often, this includes a different propagation path. It is desirable that the different propagation paths are uncorrelated such that any shadowing or fading occurring on one path will not likely occur on the other. This way, adequate signal strength is consistently maintained at the receiver.

Some method of diversity is usually found in any outdoor wireless system. There may be diversity in frequency assignment, temporal assignment, and space. Macro-diversity is attempted in order to reduce the effects of large-scale variations whereas micro-diversity is used to mitigate the effects of small-scale variations.

By allowing this diversity, a significant performance enhancement has been found to result [32]. For example, the use of base station diversity were reported to increase coverage by as much as 14% [11].

This work is concerned with a form of macro-diversity called spatial diversity. That is, each subscriber will home in on the base station to which the propagation path is attenuated the least. A subscriber in cell 'A' may home in on a base station located in cell 'B' if the path loss endured to cell 'B' happens to be less than that experienced to cell 'A'.

Thus, diversity is essential for LMCS providers to achieve maximum coverage despite the formidable propagation challenges. Combining diversity applications with the use of repeaters will increase coverage in especially difficult environments.

3.5 Power Control

As interference significantly impacts the performance of any cellular radio network, the output power of transmitters is usually controlled. This control ensures that each transmitter only uses the minimum power necessary to establish and maintain an adequate communication link. In turn, this reduces overall power consumption and greatly diminishes interference levels at both the subscriber and base station antennas.

Power control can be used to directly combat the *near-far problem*. That is, if no power control scheme exists and all subscribers transmit with the same power, then subscribers close to the base station will saturate it and essentially block out subscribers

further out in the cell. When power control is exercised, the subscriber near to the base station is ordered to lower its transmit power to a level at or just above the minimum necessary to maintain an adequate link. Likewise, the subscriber farther out from the base station is ordered to increase its transmit power to a level such that the receive power is maintained at an adequate level.

However, a base station is unable to control the power of a subscriber in a neighbouring cell that may be interfering with its communications [15]. This is why a power control scheme combined with the use of highly directional antennas will experience the best possible system performance. Power control can also be used in TDMA and CDMA systems, but it is more critical to CDMA systems. Finally, power control can also reduce ACI.

Chapter Four

FIELD MEASUREMENTS

This chapter describes the field measurements that were taken in the community of Glebe in the city of Ottawa. These measurements were conducted throughout the months of August and September of 1999. The measurement plan and the equipment used to gather the measurements are described. Next, an explanation of the methods used to process the raw data and extract the propagation parameters is provided. Finally, the results of the measurements along with their implications on LMCS design are discussed.

4.1 Measurement Plan

Due to a general lack of a substantial amount of field measurements in higher frequencies, it was decided to obtain a series of measurements in an urban area of Ottawa. The Glebe was chosen due to its age relative to other newer, less developed communities. It is a well-established community with tall, older buildings, and large trees. The measurements were taken in the summer when the trees were in full foliage causing the maximum attenuation. This way, results will indicate a worst-case propagation scenario and any LMCS design which compensates for this propagation environment will likely have the best possible coverage at other times during the year.

The transmitter was placed on the roof of Glebe High School that stands 20 metres above street level. Figure 4.1 shows two views from the roof of the high school and the general propagation environment. Most houses in the Glebe are at least two

stories tall, and the tree tops are at or above the roofs of the houses. In the bottom view of Figure 4.1, there is direct LOS with the closest row of houses, but trees impede the LOS in the very next row. This is typical of the Glebe community and would impose a challenging propagation situation on any potential LMCS provider.

Figure 4.1 Glebe Community

The transmitter was mounted on a one metre tall tri-pod. The antenna of the transmitter was slightly declined so as to maximize the footprint of the signal. This declination was consistent for all measurements. A compass was used to align the transmitter to each desired bearing (with the transmitter off).

At each measurement site, the receiver was placed on a card table that stood one metre above the ground. Usually, the table was levelled on the sidewalk. For consistency of measurements, the receiver was level with the street at all sites and the highest possible receive power was found by moving around a small area in each chosen site.

The fact that the receiver was level with the ground caused the received signal to experience less than the maximum antenna gain at short T-R distances (< 200 m); a lesser antenna gain was actually applied to the received signal power. However, the elevation correction applied during data analysis calculated the elevation angle and applies the corresponding antenna gains for each measurement site thereby yielding a true indication of path loss.

The narrow beam width of the continuous wave (CW) transmitter and receiver dictated the necessity to take measurements at a single bearing (relative to the transmitter) but at various ranges. After the signal dropped below the noise floor, the transmitter was set to a new bearing and the measurements were taken along this new path.

Each measurement consisted of a reading from the Data Acquisition Card in the Laptop. This reading was a value between 0 and 5 volts. A program written in Labview by Nausheen Naz was used to automatically tune the receiver to the maximum received power level by ramping the DC off-set of the receiver from 0 to 5 volts. The DC off-set at the maximum received power was used for each measurement.

For each measurement site, 10 readings were recorded. After a single reading was taken, the receiver was moved at least 10 cm, at which point the next reading was taken. The moving of the receiver was done so that the effects of multipath fading could be averaged out. Papazian, et al, [10] provide justification for such a procedure based on the random nature of obstructions to the propagation path. Presumably, moving the receiver a few wavelengths will change the phases of all scattered components. The received signals from different positions separated by a few wavelengths will be uncorrelated. Thus, a mean of several such measurements will average out the effects of all various obstructions located in the vicinity of each receiver site and will yield a homogeneous estimate of the path loss between the transmitter and that measurement site. A similar method was conducted by Durgin, et al, but at a lower frequency (5.85 GHz) [33].

4.2 Equipment

The CW equipment used for the field measurements consisted of a transmitter, receiver, battery, and laptop computer equipped with a data acquisition card. It was constructed by Robert Hahn, in a joint CRC and Carleton University project. Complete specifications are provided in [34], but the following section is presented as a brief overview with all the necessary information of relevance to this work.

4.2.1 Transmitter unit

The transmitter unit consists of two identical Gunn oscillators each feeding a waveguide circulator, a three inch length of waveguide, and a linearly polarized antenna. Figure 4.2 shows the basic configuration of the transmitter. The waveguide of one of the oscillators has a 90 degree twist to provide a vertical E-field polarization in one antenna and a horizontal E-field polarization in the other antenna. Both oscillators have been adjusted to operate at a frequency of 29.5 GHz after the warm-up period. The antennas of the transmitter unit are two Flann conical horn antennas with a maximum gain of 28 dBi (as shown in Figure 4.5). There is a dummy load on each transmitter to limit the output of the transmitter so it is safe for indoor use by providing a 25-30 dB attenuation resulting in a 20 dBm output power. Thus, the transmitter will produce an EIRP of 48 dBm (20 dBm output power + 28 dBi antenna gain). Note that only the vertical polarization antenna was used as LMCS typically uses vertically polarized antennas.

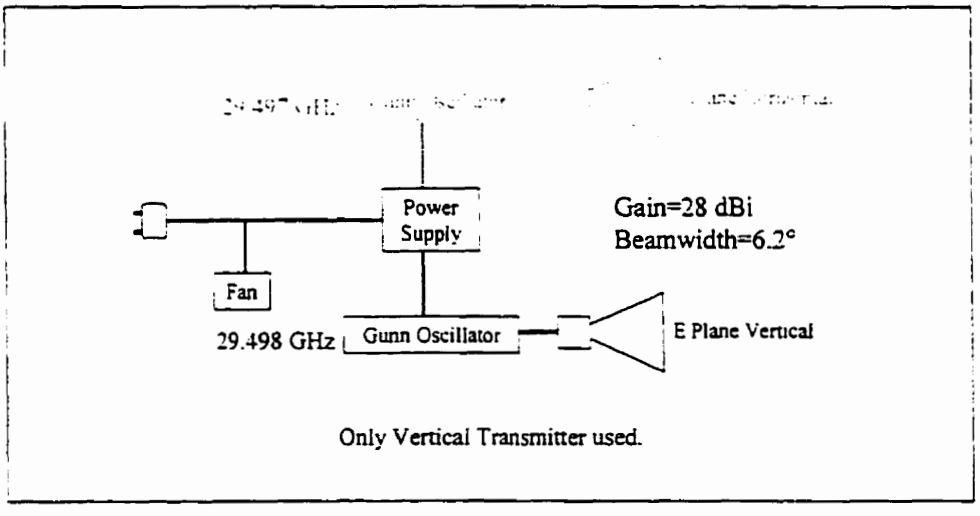

Figure 4.2 CW Transmitter Block Diagram

4.2.2 Receiver unit

The receiver unit consists of a 27-30 GHz, 6.2 degree, Flann conical horn antenna, power supply input, IF loop, and a Personal Computer Memory Card International Association (PCMCIA) interface connector. Figure 4.3 shows the receiver configuration. A power supply of between 10 to 17 volts at less than 0.7 amps is required for proper functioning of the receiver unit. A commercial car battery was employed for this purpose. Note that it required recharging after each day's measurements to stay within the power requirements of the receiver.

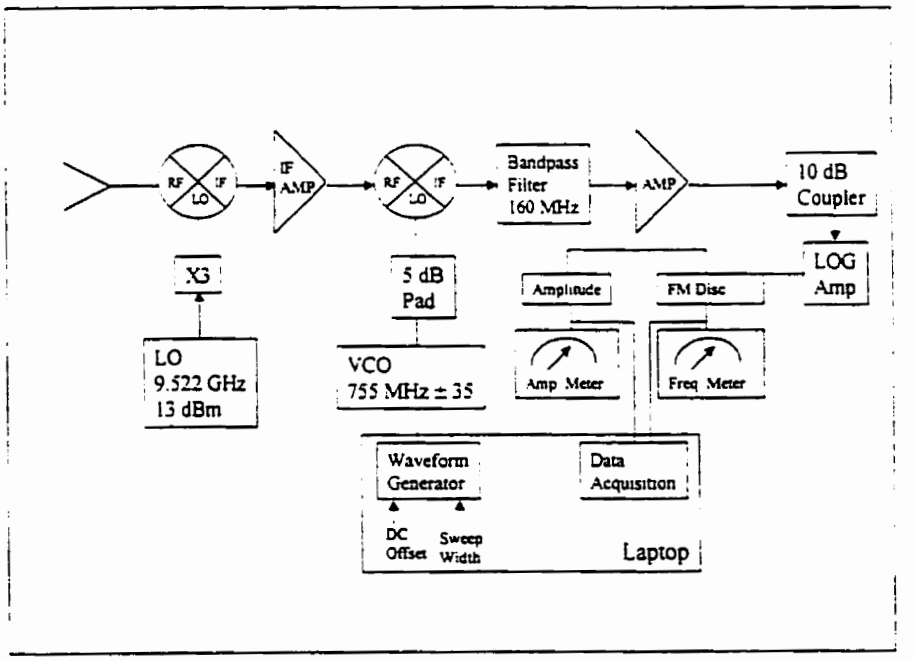

Figure 4.3 CW Receiver Block Diagram

4.2.3 Laptop/DAQ card

The output of the receiver was sent through an interface into a PCMCIA Data Acquisition (DAQ) card installed in a 166 MHz Pentium Laptop computer. A data

acquisition software called, LabView, was used to control the receiver, record measurements, and output them to a binary file. The DAQ card has a 12-bit analog-to-digital converter and both the sampling rate and duration of samples could be adjusted. However, for the purposes of these measurements, a sample value was all that was required. Tuning of the receiver was accomplished by the LabView program as well. A ramp of the DC offset was performed and set to the resultant maximum received voltage.

4.2.4 Link Budget

The CW equipment has the following link budget. The effective isotropic radiated power (EIRP) is calculated from the transmitter power and the transmitter gain according to:

$$EIRP = P_t + G_t \tag{4.1}$$

The transmitter power is 20 dBm and using the maximum antenna gain of 28 dBi, the EIRP is 48 dBm. The free space path loss is given by [12]:

$$FSPL = \left(\frac{4\pi d}{\lambda}\right)^2 \tag{4.2}$$

Rewriting Equation 4.2 to provide an expression for the free space path loss at distance d yields the following expression in units of dB:

$$FSPL = 32.44 + 20\log_{10} d + 20\log_{10} f \tag{4.3}$$

where: d is the T-R distance in km, and

f is the frequency in MHz.

For example, at a distance of 1 km, the FSPL is 122 dB.

The received signal level (RSL) is defined as:

$$RSL = EIRP - FSPL + G_r - Lineloss \tag{4.4}$$

Using the maximum possible receiver antenna gain of 28 dBi and a lineloss of 6 dB, the RSL is –52 dBm.

Next, the noise floor (NF) of the equipment is calculated according to:

$$NF = -174 + NoiseFigure + 10\log_{10}(IFBW) \tag{4.5}$$

where: IFBW is the IF bandwidth of the equipment.

The Noise Figure for the equipment is 2 dB, and the IF bandwidth of 4 MHz, which result in a Noise Floor for the CW equipment of –106 dBm.

Thus, from the RSL and the NF, the signal to noise ratio (SNR) can be calculated:

$$SNR = RSL - NF \tag{4.6}$$

Continuing the previous example, for a T-R distance of 1 km, the SNR is:

$$\text{SNR} = -52 - (-106) = 54 \text{ dB}$$

For the range of distances encountered in the measurements, the free space SNR varies from 74 dB at 100 m to 48 dB at 2000 m.

4.3 Analysis

This section describes the methods used to analyse the measurement data and present it in a meaningful way. As previously mentioned, the raw data was stored in

binary files that required conversion. A correction was applied to the data to correct for the different antenna gains experienced at small propagation distances.

4.3.1 Data Analysis

The resulting data collected from the field consists of 10 separate received power measurements per measurement site. The analysis of the data began with converting each measurement from Volts to dBm. A lookup table was constructed for this purpose from the calibration curve found in Figure 4.4. The curve was included in the CW Propagation Test Set [34].

After each measurement was in units of dBm, they were then converted to milliwatts for the purpose of averaging each group of 10 measurements, resulting in the mean received power for each measurement site. These averages were then converted back into units of dBm.

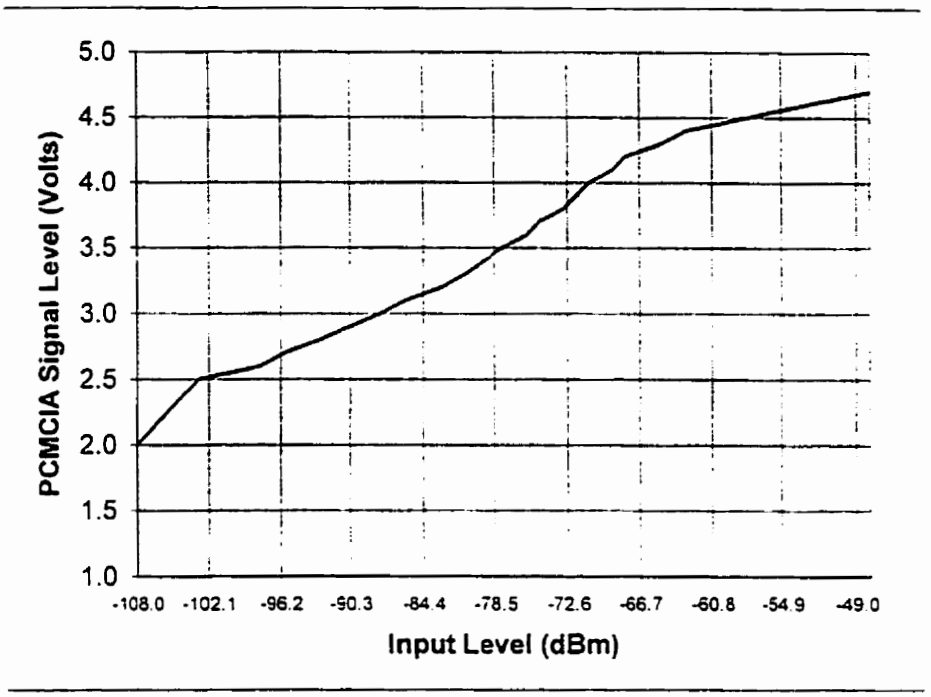

Figure 4.4 CW Equipment Calibration Curve

4.3.2 Elevation Correction

It is necessary to apply an elevation correction after all the data has been complied to account for the antenna pointing loss. That is, the elevation correction compensates for the fact that the antenna beam pattern and hence, antenna gain, is significantly lower at the higher elevation angles expected at small T-R distances. The closer the measurement site is to the transmitter, the further away the receiver will be from the centre of the antenna beam and therefore less antenna gain will be in effect by both the transmitter and receiver.

The following graph in Figure 4.5 shows the antenna beam pattern. The gain of the antenna is plotted on the vertical with the horizontal representing the elevation angle. Both the transmitting and receiving antennas used were conical and therefore the antenna gain was symmetrical for both the horizontal and vertical axes. The maximum gain of 28 dBi is at an elevation angle of 0°.

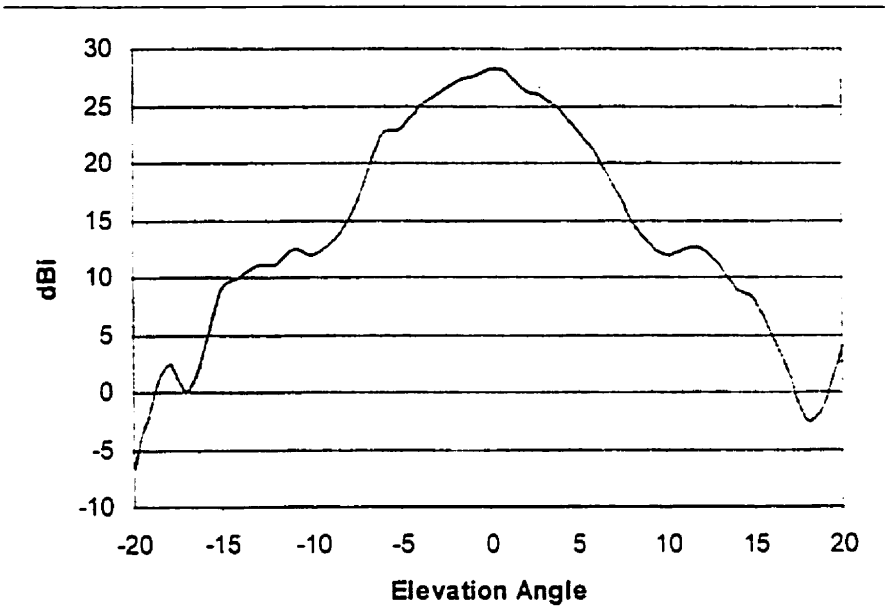

Figure 4.5 CW Equipment Beampattern

The formula used to calculate the elevation correction is:

$$\theta_{rx} = \tan^{-1}(\frac{y}{x}) \tag{4.7}$$

$$Pathloss = [P_t + G_t] - [P_r - G_r] \tag{4.8}$$

where: θ_{rx} is the elevation angle according to the diagram in Figure 4.6,

y , x are the distances as indicated in Figure 4.6 Note that the elevation of the measurement site as well as the height of Glebe High School are accounted for in y,

G_t, G_r are the gains of the transmitter and receiver, respectively. Note that the calculated elevation angle is converted into the gains according to the beam pattern shown in Figure 4.6, and

P_t, P_r are the transmitted power and the received power, respectively. A value of 20 dBm was used throughout for the transmitted power [34].

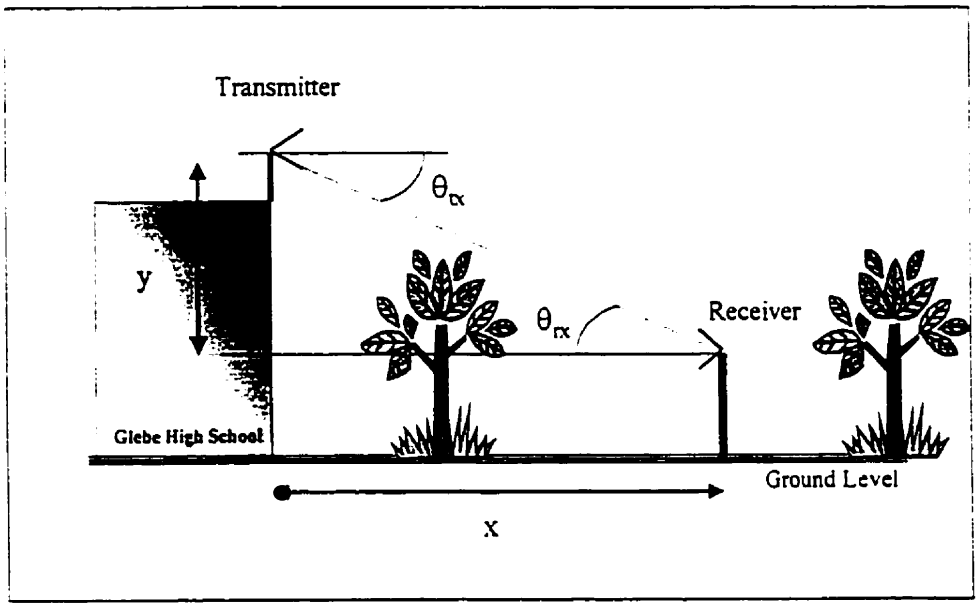

Figure 4.6 Elevation Correction

A sample calculation of the elevation correction is as follows:

T-R Distance: 175 m Height of Receiver: 1 m

Received Power: -57.4 dBm Height of Transmitter above rooftop: 1 m

Height of Glebe High School Rooftop: 20 m

Elevation of Glebe High School: 80 m

Elevation of Receiver Site: 80 m

The angle calculation is:

$$y = 20\text{-}1 \div 80\text{-}80 = 19 \text{ m} \qquad x = 175\text{m}$$

$$\theta_{tx} = \theta_{rx} = \tan^{-1}(19/175) = 6.20°$$

Looking up 6.20° in the beam pattern chart (Figure 4.5) yields a receiver gain of 21 dB and transmitter gain of 18 dB. Therefore, the final path loss calculation is:

$$\text{Pathloss} = [20 + 18] - [-57.4 - 21] = 116.4 \text{ dB}$$

Thus, the elevation correction has the greatest effect on the measurements taken at small T-R distances resulting in a significantly altered path loss slope and a corresponding higher path loss exponent.

4.4 Results

The results of the measurements are contained in this section. Firstly, a description of the measurements sites is provided with the reasoning behind their choice. Next, the raw data and the processed data is presented with out the elevation correction applied. The results with the elevation correction applied are subsequently shown. Finally, a comparison is made with results from other sources followed by a discussion.

4.4.1 Measurement Sites

A total of 80 measurement sites were completed. These sites were distributed in 12 slices, or series of measurement sites at a single bearing. Figure 4.7 shows the measurements sites radiating out from the transmitter location of Glebe High School. The proximity of the Queensway (Highway 417) made measurements sites north of the high school problematic.

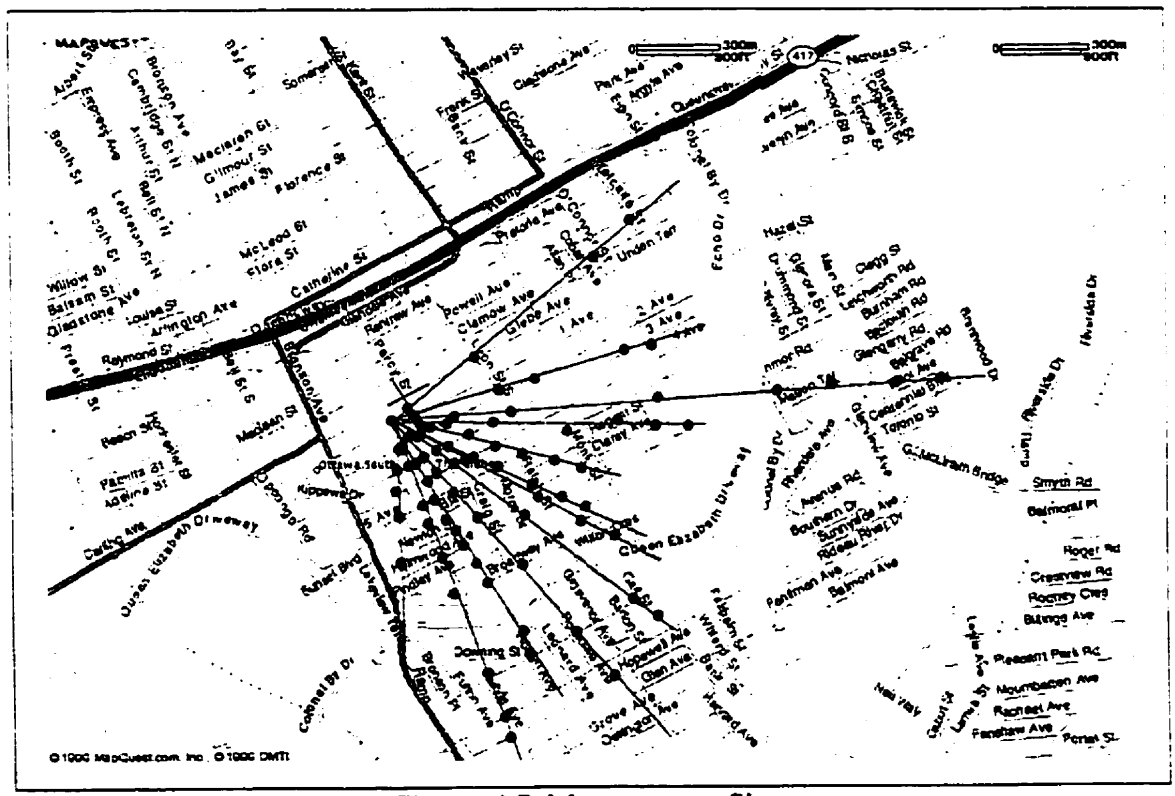

Figure 4.7 Measurement Sites

The map shown is reproduced with permission from Mapquest.com, Inc. and was found on the website: www.mapquest.com.

Some bearings have more measurements than others due to the fact that potential sites were not readily available at discrete ranges. Thus, for a single bearing, sites were chosen at locations where there was room to set up the receiver with no regard for the range. It was thought that enough measurements would cover a sufficient number of ranges yielding an accurate measurement of the propagation parameters.

4.4.2 Uncorrected Results

The raw, unprocessed measurement data is shown in Figure 4.8. Recall that each point represents an average of 10 measurements at a single site. Several measurement sites did not receive a detectable signal through the noise. The abundance of measurements at –106 dB coincides with the noise floor of the CW equipment.

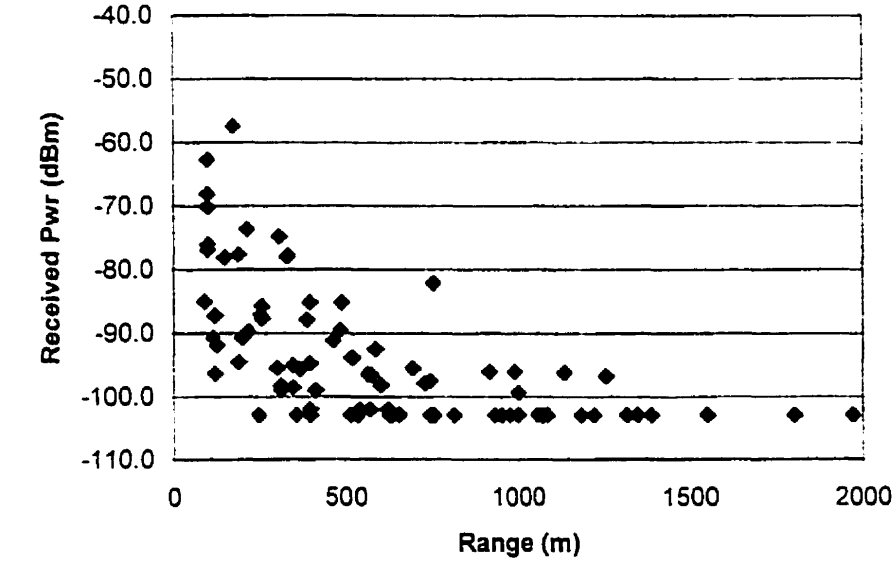

Figure 4.8 All Measurement Data

Applying the Equation 4.8 yields the results in Figure 4.9 when the maximum antenna gain (28 dBi) is used for both transmitter and receiver. Data is plotted in an x-y graph with the x-axis being logarithmic. This is done so that the propagation exponent can easily be extracted from the slope of the graph according to the following equation:

$$PL = 10n\log_{10}(r) \quad (dB) \tag{4.9}$$

where: PL is the path loss in dB,

n is the propagation exponent, and

r is the T-R range in metres.

Thus, a slope of −17.80 in Figure 4.9 corresponds to an propagation exponent of 1.78 which is much lower than expected and is even lower than that predicted by the free space path loss model. However, this pathloss is calculated with 28 dBi antenna gains, which was not, in actuality, always the case.

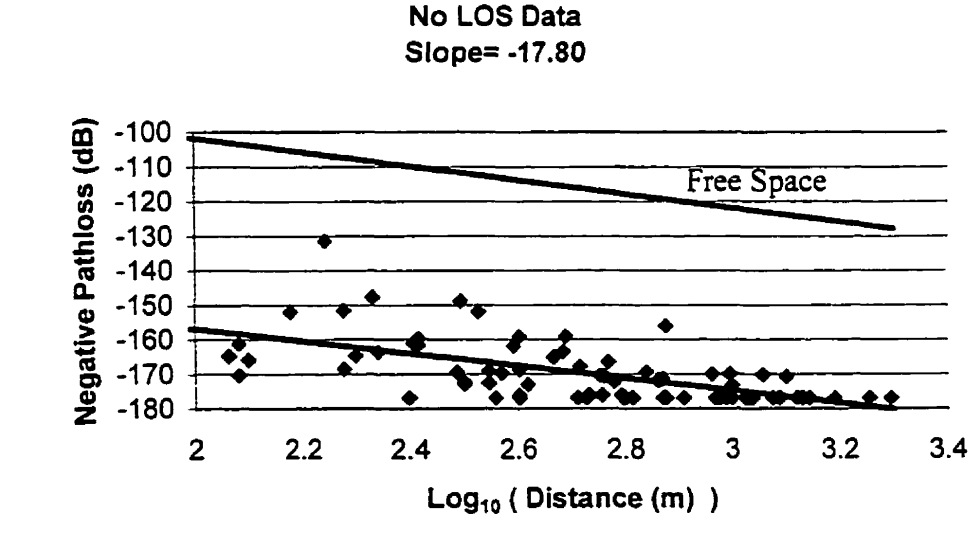

Figure 4.9 Uncorrected Pathloss

Data taken from sites very close to the transmitter (< 200 m) that enjoyed LOS propagation paths was removed in Figure 4.9; there were six LOS measurements out of 80. This was done to ensure a homogeneous series of measurements; all NLOS.

The line shown in the measurements represents the linear regression fit of the data. The other line represents the free space path loss curve was plotted with Equation 4.2. Note the abundance of measurements near the noise floor of the equipment (-184 dB, including antenna gains). There were 28 out of 80 measurements which were at the noise floor. They partially account for the observed path loss exponent to be less than that of free space (slope=2).

The standard deviation of the data shown in Figure 4.9 is 9.01 dB. This is near the expected value of 10 dB.

4.4.3 Corrected Results

The data with the true elevation correction applied is shown in Figure 4.10. The data at or below the noise floor is removed along with the data taken from sites with direct LOS. The noise measurements are also removed so that a path loss exponent can be derived from true measurements.

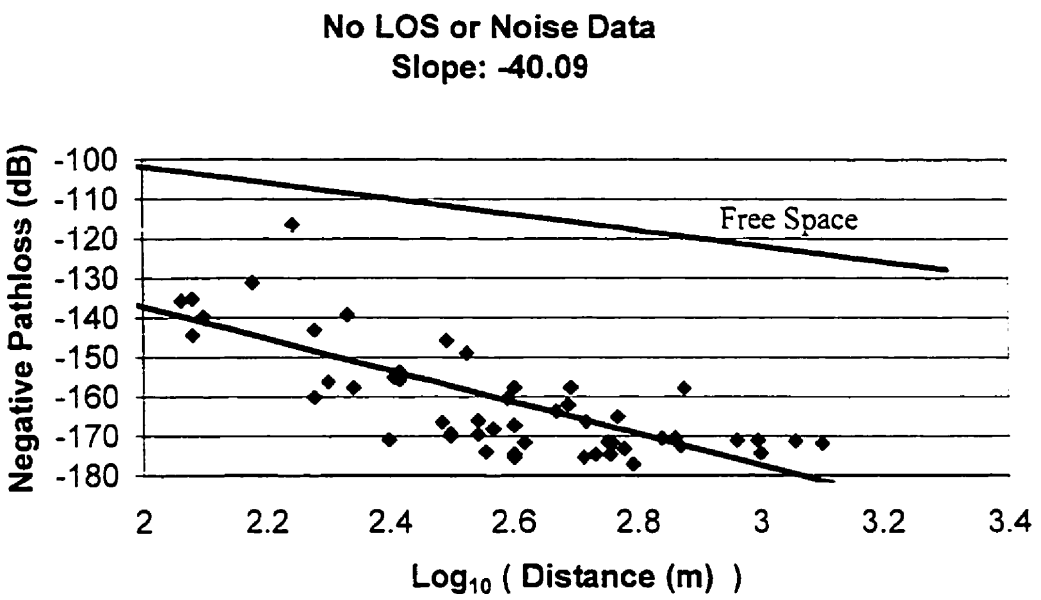

Figure 4.10 Corrected Pathloss

The slope of the corrected graph has decreased, indicating an observed propagation exponent of 4.01. The standard deviation of this data was 13.89 dB indicating a fair degree of shadowing was encountered.

Thus, applying the elevation correction has made a dramatic difference on the results by reducing the perceived path loss at short T-R distances. A propagation exponent of 4.01 is consistent with ground plane theory [15].

4.5 Results from Other Sources

This section reviews results reported in other sources. This is done to show that similar results have been reported and thus adds validation to the field measurements.

Propagation measurements were carried out by CITR in 1996 and 1997 in the area of Parkwood Hills, Ottawa [35]. Parkwood Hills is a community comparable to the Glebe in terms of propagation considerations. These measurements were also continuous wave (CW) but at a frequency of 28.5 GHz and at roof level. A propagation exponent of 5.0 was found for the NLOS measurements. The standard deviation of log-normal shadowing was found to be 14 dB.

Seidel and Arnold reported another series of similar propagation measurements [13]. These measurements were taken at 28 GHz in Brighton Beach, a built-up area of Brooklyn. This investigation found signal strengths much weaker than that predicted by free space propagation despite using an antenna height of 11.3 metres above ground level. A clear dependence of signal level on both the azimuth angle and receiver antenna height was demonstrated. These results also suggest that energy at angles other than that of bore-sight could potentially fill coverage gaps.

4.6 Discussion

The results of the propagation measurements in this work were largely consistent with those reported by other sources. Bultitude, et al, observed a propagation exponent of 5.0 whereas this work found a smaller 4.0 propagation exponent.

The standard deviation reported by Bultitude, et al, was about the same as that observed by the measurements in the Glebe. However, those measurements were conducted with the receiver at roof level whereas the measurements reported here were at

ground level. This number of obstructions encountered at roof level is likely to be much less than that encountered at ground level. Thus, a lesser shadowing deviation is expected for measurements at roof level.

Before the measurements were taken, several sites were checked for the presence of interference. The transmitter was turned off, and the receiver was set up at various sites to determine whether or not there were interfering signals. However, no interference of any kind was detected.

Some research [35] suggests that a breakpoint may exist in the path loss at a particular distance. That is, a propagation exponent will be present up until a certain distance, the breakpoint, after which a greater propagation exponent could exist. However, Correia, et al, suggest the breakpoint may exist outside the typical LMCS cell radius [6]. Due to the sensitivity limitations of the CW equipment used in this research, a break point was not observed.

The exclusion of the data below the noise floor may lead to a biasing effect on the perceived coverage of these propagation measurements. Technically, the lack of a received signal power indicates a hole in the coverage at that site. By excluding the data, the measurements only indicate the propagation exponent and standard deviation of the measurements above the noise floor. Thus, care should be taken when considering coverage implications of this fieldwork.

4.7 Summary of Results

There were 80 measurements in total. Of them, six were LOS and 28 were at the noise floor of the equipment leaving only 46 measurements for inclusion in the final results.

A path loss exponent of 4.01 was observed after the LOS and noise data was removed and an elevation correction was applied. The standard deviation of the processed data was 13.89 dB. These results were found to be consistent with those reported in other sources.

Chapter Five

INTERFERENCE AND SHADOWING MODEL AND ANALYSIS

This chapter introduces a theoretical model from which a simulation is constructed. A description of the model parameters and the underlining theory is followed by the simulation results. The simulation was constructed using a MATLAB program on a Pentium II 300 MHz computer that was found to be adequate computational power for the simulation.

Results from the field measurements are used to construct the predicted path loss of the simulation. Specifically, the path loss exponent and standard deviation of log-normal shadowing measured in Chapter 4 are parameters in the simulation. It is hoped that a more accurate model of the interference in a LMCS system will result.

5.1 Model Parameters

This section provides the theoretical basis for the simulation and the parameters that comprise it. A general model of interference in an LMCS network is presented followed by the specifics of the parameters of the simulation to be tested. Propagation loss, log-normal shadowing, antenna beam patterns, hub sector size, and base station diversity are all components of the simulation and the method of modelling them is described.

5.1.1 Interference Outage

With reference to Figure 5.1, an interferer "j", which homes on a particular base station BS(j), interferes with all other base stations i= 0, 1, 2, ... (i≠j), and must have a maximum received power at BS(j), to home on it.

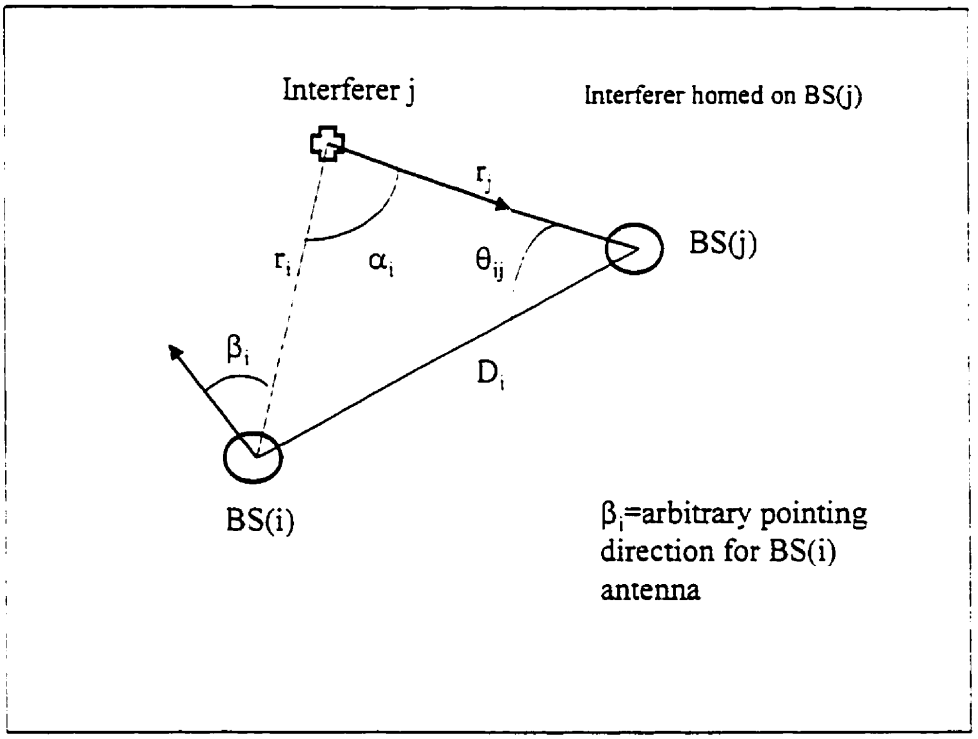

Figure 5.1 Interference Outage

The interferer transmits power P_t (dBm). The average path loss over distance r can be modelled as:

$$p(r) = -A - B \log_{10} r \text{ (dB)} \tag{5.1}$$

Including log-normal shadowing, the actual path loss is:

$$= p(r) - \chi \text{ (dB)} \tag{5.2}$$

where: χ is a zero-mean Gaussian random variable with standard deviation of σ that represents the log-normal shadowing over the path. Then the power received from the interfering subscriber at its own base station BS(j) is:

$$P = P_t - p(r_j) + \chi_j + G_S(0) + G_B(0), \tag{5.3}$$

where: $G_S(0)$, $G_B(0)$ are the bore-sight gains of the subscriber and base station antennas, respectively. Actual bore-sight gains would be typically 10-15 dBi for a 90° sector base and about 30 dBi for the subscriber. If power control is used, P is fixed for all transmitters at their own base stations, so:

$$P_t = P - p(r_j) - \chi_j - G_S(0) - G_B(0) \tag{5.4}$$

The power from the given interferer, which is received at the victim base station BS(i), assuming perfect power control, is:

$$I_i = P_t - p(r_i) + \chi_i + G_s(\alpha_i) + G_B(\beta_i) \tag{5.5}$$

Substituting Equation (5.4) yields:

$$I_i = P + p(r_j) - p(r_i) + \chi_i - \chi_j + G_s(\alpha_i) + G_B(\beta_i) - G_s(0) - G_B(0) \tag{5.6}$$

where: χ_j is another zero-mean independent Gaussian random variable representing shadowing occurring on the path between the interferer and base station j, with standard deviation σ,

$G_s(\alpha_i)$ is the interferer's antenna gain in the direction of BS(i),

$G_B(\beta_i)$ is the base station's antenna gain in the direction of the subscriber that is homing on it.

Base station diversity is modeled as follows: for the interferer to home on BS(j), a necessary condition is:

$$p(r_i) - \chi_i \geq p(r_j) - \chi_j \qquad \text{for all } i \neq j \qquad (5.7)$$

or

$$\chi_i - \chi_j \leq p(r_i) - p(r_j) \qquad \text{for all } i \neq j \qquad (5.8)$$

Note that the greater the degree of shadowing that occurs on the radio paths, the more likely it is for the interferer to home in on a base station other than the one closest to it. That is, the greater the standard deviation of the log-normal shadowing, σ, the more likely it is that a path to another base station endures less path loss than the one closest to the interferer. For modelling purposes, σ is set to 10 dB, unless otherwise stated.

5.1.2 Simplified Interference Model

This section introduces a simplification in the model to reduce the number of calculations required in each run of the simulation, thereby reducing the run time. Assuming there is exactly one subscriber homing in on any base station at a given frequency, then each such subscriber will interfere with all the other base stations. The total interference at any base station will be the sum of its received powers, through its antenna, from all subscribers that are homing on other base stations.

The following observation is the basis of a simplified interference model that we subsequently use: the statistics of the total interference at any one base station, from all other subscribers, will be the same as those of the sum of all interference $\{I_i\}$ at base

stations $\{BS(i)\}_{i \neq j}$ from interferer j, which homes on the j^{th} base station, if statistical averaging is carried out over all possible positions of j and if all base stations except BS(j) have the same pointing direction for their antennas. With respect to Figure 5.2, let j=0, and number the other base stations i=1, 2, 3, ...

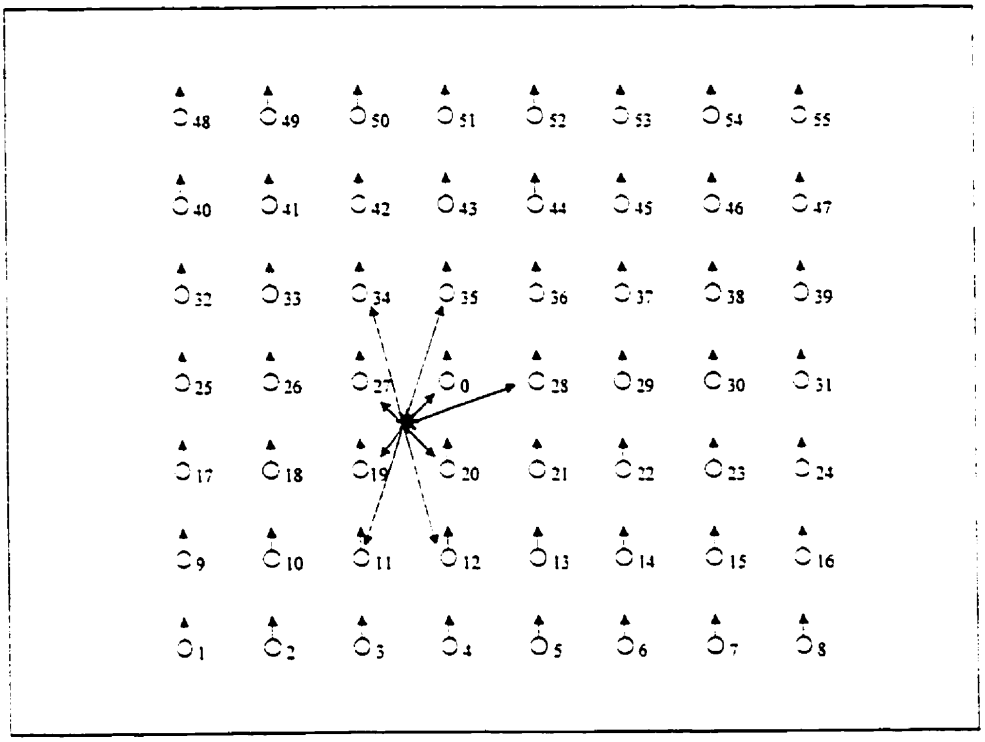

Figure 5.2 Interference Model

$\sum_{i=1}^{N-1} 10^{\frac{I_i}{10}}$ has the same statistics as the total interference from all interferers (one per base station) at a given base station. N is the total number of base stations in the network. So, the total interference random variable is:

$$\text{Total Interference} = \sum_{i \geq o} 10^{\frac{I_i}{10}\phi_i(\{r_l\},\{\chi_l\})} \tag{5.9}$$

for a fixed interferer position, where an indicator function is used:

$$\phi_i(\{r_l\},\{\chi_l\}) = \begin{cases} -\infty & \text{if} \quad p(r_i) - \chi_i \leq p(r_l) - \chi_l \quad \text{for all} \quad l \neq i \\ 1 & \text{otherwise} \end{cases} \tag{5.10}$$

or, written more simply:

$$\phi_i(\{r_l\},\{\chi_l\}) = \begin{cases} -\infty & \text{for} \quad i = \arg\min\{p(r_l) - \chi_l\} \\ 1 & \text{otherwise} \end{cases} \tag{5.11}$$

The purpose of the indicator function is to model base station diversity by determining which received power is interference and which received power is signal. That is, the incoming signal from the subscriber homed to a base station is not interference to that base station.

Defining a new variable y:

$$y_i \equiv p(r_i) - \chi_i = -A + B \log r_i - \chi_i \qquad \text{(dB)},$$

which is a Gaussian random variable with variance σ^2 and mean equal to: $p(r_i) = -A + B \log_{10} r_i$. Then for the case of ideal power control,

$$I_i = P + y_i - y_i + G_s(\alpha_i) + G_B(\beta_i) - G_s(0) - G_B(0) \tag{5.12}$$

and the total interference random variable for a given interferer position

$$\text{Total Interference} = \sum_{i \geq o} 10^{[\frac{1}{10}[P + y_j - y_i + G_s(\alpha_i) + G_B(\beta_i) - G_s(0) - G_B(0)]]\phi_i(\{y_l\})} \tag{5.13}$$

$$\text{where: } \phi_i(\{y_l\}) = \begin{cases} -\infty & for \quad i = \arg\min\{y_l\} \\ 1 & otherwise \end{cases} \tag{5.14}$$

Re-writing the indicator function as the minimum of all the random variables $\{y_l\}$, Equation 5.13 becomes:

$$\text{Total Interference} = \sum_{i \neq \arg\min\{y_l\}} 10^{\frac{1}{10}[P + \min\{y_l\} - y_i + G_s(\alpha_i) + G_B(\beta_i) - G_s(0) - G_B(0)]} \tag{5.15}$$

The signal to interference ratio (SIR) will be simply:

$$\text{SIR} = \frac{P}{\sum_{i \neq \arg\min\{y_l\}} 10^{\frac{1}{10}[P + \min\{y_l\} - y_i + G_s(\alpha_i) + G_B(\beta_i) - G_s(0) - G_B(0)]}} \tag{5.16}$$

In summary, the signal to interference ratio of a LMCS network will be calculated using Equation 5.16. Testing the computed SIR against a SIR threshold will render a probability of outage, which is used to gauge the system performance. The simulation will be used to evaluate the several factors to determine their effect on interference contributed by the single subscriber.

5.1.3 Model Geometry

A graphical representation of the model is shown in Figure 5.3. The square cellular geometry was chosen for programming convenience. A hexagonal geometry may be slightly more accurate in terms of the area covered by each cell, but since base station diversity is incorporated into the model, which particular cell the subscriber happens to be in does not affect the outage probability.

When distances are calculated in this model, they are scaled so that a model distance of 1.0 becomes 1000 m for path loss calculations.

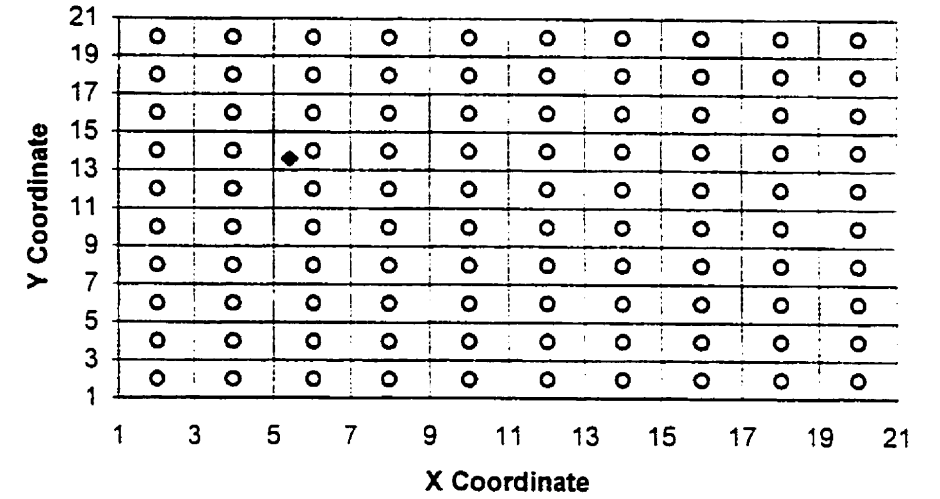

Figure 5.3 Single Subscriber Model Geometry

The interferer shown at coordinates (5.5, 13.5) is an example. For each run of the simulation, a new subscriber position is randomly chosen on the model area.

Bearing calculations are used in the simulation to compute the antenna gains. When the base station that the interferer homes on is chosen, the direction of the interferer's antenna is set. As shown in Figure 5.4, all base station's antennas are pointed in an arbitrary direction – in this case, 90°. To calculate the gain of the interferer's antenna in the direction of a base station, a bearing from the interferer to that base station is calculated using their respective coordinates. Next, the simulation decides if that

bearing is within the beam width of the interferer's antenna. If it is, then the high gain is applied, otherwise the lower gain is used.

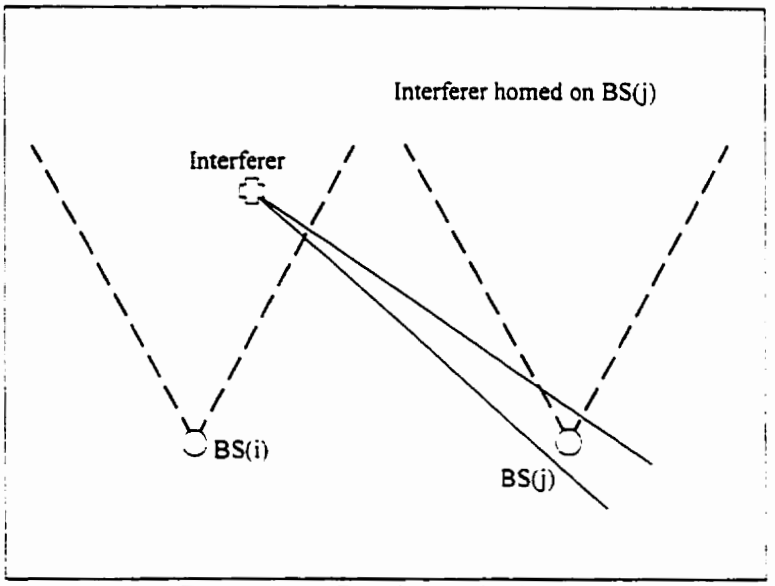

Figure 5.4 Bearing Calculation

A similar operation is conducted to determine the gain of the receiver at the base station that is applied to the direction of the interferer.

5.1.4 Propagation Model

As discussed in section 5.1.1, the path loss is modelled according to the following equation:

$$\text{Path Loss} = A\text{-}B \log_{10} r \qquad (5.17)$$

The values used in the forthcoming simulation vary according to what the simulation is designed to show. The parameter 'A' is set to zero for all simulations since it is always cancelled in the computation of the total interference with Equation 5.15.

The parameter B will be varied to determine their effect on the expected total interference. Setting B to a value of 40 corresponds to simulating a propagation exponent of 4.

The effect of log-normal shadowing on the interference level present in an LMCS network will be shown by varying the standard deviation of log-normal shadowing and determining the average total interference statistic that results with each change in standard deviation. The expected effect is for each increase in standard deviation, a corresponding increase in the standard deviation of the resulting distribution of interference powers.

5.1.5 Antenna Beam Patterns

The antenna gain patterns are modeled as two-valued shown in Figure 5.5. The beam width is defined as the angle over which the high gain is applied.

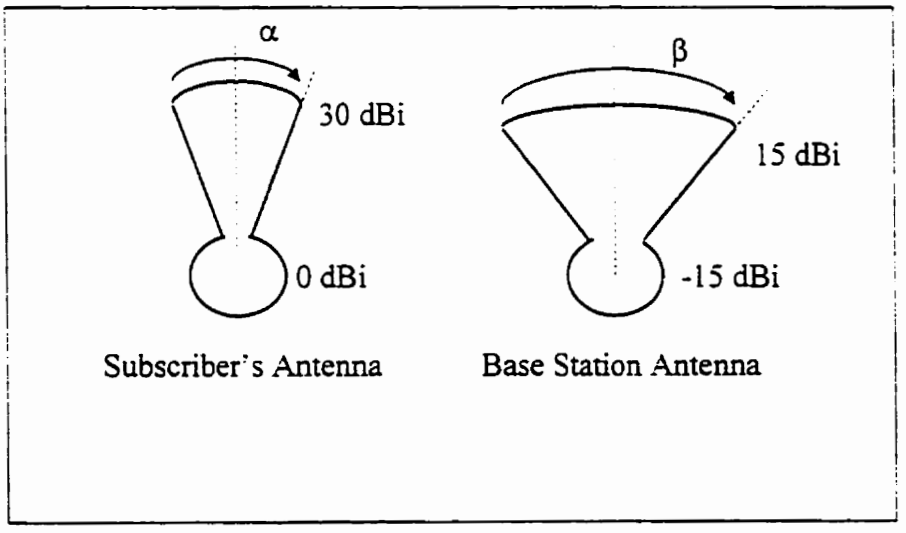

Figure 5.5 Model Antenna Beam Patterns

The beam width of both the interferer and base station's antennas will be varied to determine their effect on interference levels. It is expected that increased beam width will correspond to higher interference levels since more interference energy will be captured with larger beam widths.

The ratio between the high gain value and the low gain value is termed the antenna gain ratio. These ratios will also be varied to evaluate their effects on interference levels and outage probabilities.

Figure 5.6 shows the realistic base station antenna beam pattern found in [16]. It is employed later to determine the validity of using the model antenna beam patterns shown in Figure 5.5. The simulation calculates the bearing from the interferer to each of the base stations to yield an angle of incidence. This angle is used to determine the gain of the base station antenna in the direction of the interferer, and vice versa.

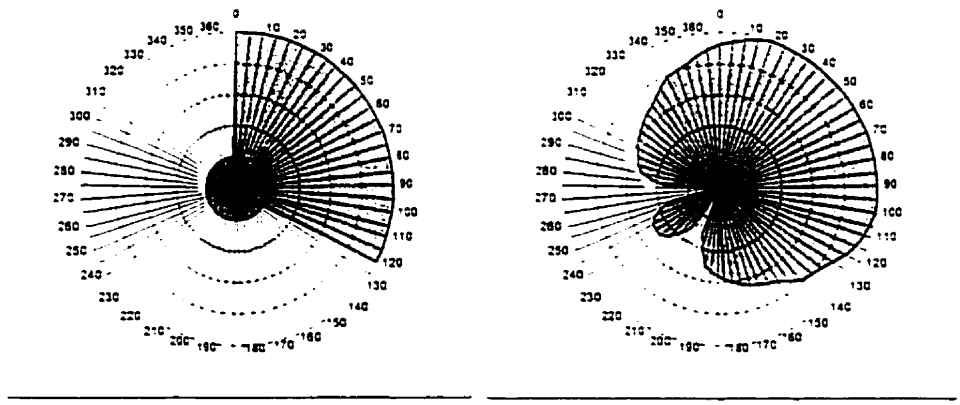

(a) (b)

Figure 5.6 Antenna Beam Patterns for 120° sectors. (a) Ideal (b) Realistic

5.1.6 Hub Sector Size

Several hub sector sizes were evaluated with the simulation. Figure 5.7 illustrates how the model was modified to accommodate different sector sizes. When the subscriber's position was chosen, the base station to which it homes is chosen as per the normal algorithm (Equations 5.7 and 5.8). However, the sector of the homed base station is assigned based upon the bearing of the subscriber to the homed base station.

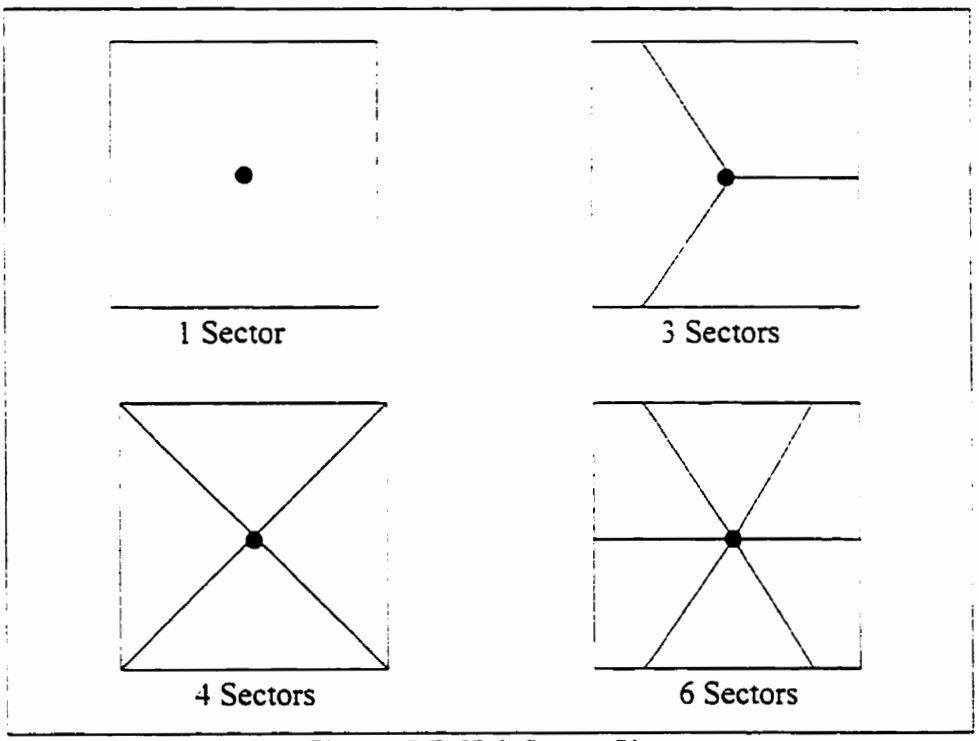

Figure 5.7 Hub Sector Sizes

A sector size of one is the situation where omni-directional antennas are used at the base stations.

5.1.7 Base Station Diversity

As previously stated, base station diversity is an integral component to the simulation. The effect of the absence of diversity will be determined by removing the condition imposed by Equations 5.7 or 5.8.

5.2 Simulation Results

This section presents the results of the simulations conducted as described in the previous sections. The effects of the simulation parameters are presented along with interpretations of their meaning with respect to LMCS interference considerations.

In this section, the parameters used in the simulation to produce the graphs are listed immediately below the graph. The parameters are:

P is the fixed signal power the interferer must achieve at its base station (dBw),

BSBW is the base station antenna beam width as indicated in Fig. 5.5,

INTBW is the interferer antenna beam width as indicated in Fig. 5.5,

BSGR is the base station gain ratio,

INTGR is the subscriber gain ratio,

n is the propagation exponent,

σ is the standard deviation of log-normal shadowing, and

N is the number of runs of the simulation that contributes to the mean interference value.

For each point on the graph, the simulation is run 10000 times. Next, for each run of the simulation, the total interference contributed by a single subscriber to the other base stations is calculated according to Equation 5.15 to render a total interference value contributed by the single subscriber. Then, the 10000 total interference values are in turn averaged (in watts) and subtracted from the fixed receive value to produce a average SIR. Then, the computed SIR is compared with the SIR threshold to calculate an outage probability. A SIR threshold of 10 dB was chosen for most simulations. A higher threshold is appropriate when considering more complex coding schemes such as QPSK.

5.2.1 Effect of Propagation Parameters

The effect of propagation exponent is shown in Figure 5.8.

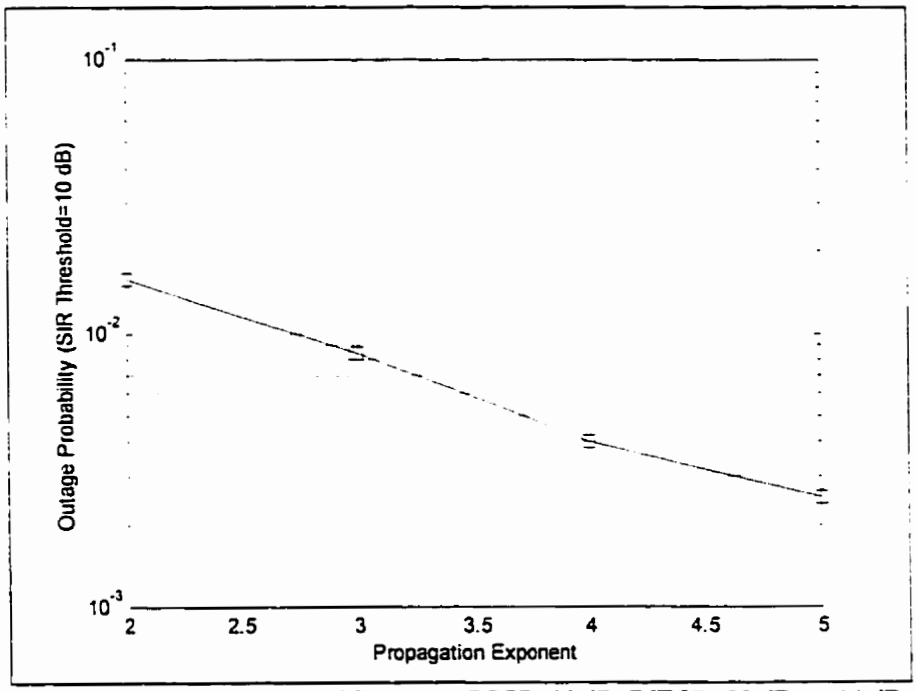

P= 30 dBw, BSBW= 120°, INTBW= 5°, BSGR=30 dB, INTGR=30 dB, σ=14 dB

Figure 5.8 Effect of Propagation Exponent

There is a distinct decrease from 1.58% to approximately 0.25% in the probability of outage with increase in propagation exponent from 2 to 5. This is due to the fact that with greater propagation exponent, the more the interfering signals are attenuated. Thus, large buildings and foliage like those encountered in the Glebe (Chapter 4) may serve to reduce the interference experienced at a base station by attenuating the interfering signals from other subscribers while at the same time attenuating the desired signals.

Note that the outage probability decreases with propagation exponent due to the neglect of thermal noise in this simulation. At larger propagation exponents, one would expect the thermal noise to cause outage.

5.2.2 Effect of Log-Normal Shadowing

Figure 5.9 show the result of the simulation when the standard deviation of log-normal shadowing is varied from 0 to 20 dB. The outage probability slowly increases until the standard deviation of shadowing reaches 10 dB, at which point the outage probability increases rapidly from 0.2% to 1.0%. Thus, log-normal shadowing has a significant effect on system performance which underscores the desirability of LOS propagation paths. Use of repeaters to avoid obstructions and reduce shadowing effects is warranted.

At $\sigma = 0$ dB, there is no outage because this simulation only computes outage due to interference, not due to thermal noise.

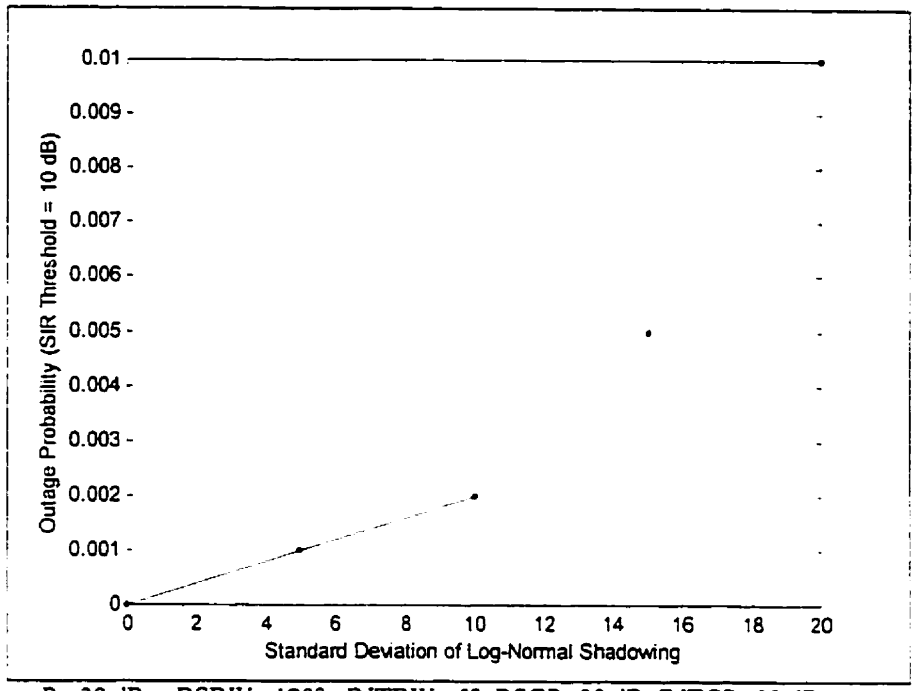

P= 30 dBw, BSBW= 120° , INTBW= 5°, BSGR=30 dB, INTGR=30 dB, n=4

Figure 5.9 Effect of Log-Normal Shadowing

5.2.3 Effect of Antenna Beam Patterns

This section contains the results of varying the different parameters associated with the interferer and base station antennas.

5.2.3.1 Effect of Antenna Beam Widths

When the interferer's antenna beam width is varied from 3° to 15°, the result is a nearly linear increase in outage probability (Figure 5.10). This is due to the fact that when the interferer's beam width is increased, it interferes with more base stations. By hitting more base stations with increased beam width and higher gain, the subscriber contributes higher levels of interference. Note that the product of the beam width and the

antenna gain of the main lobe are held constant for all beam width values so that the changes in antenna directivity are accounted for in the simulation.

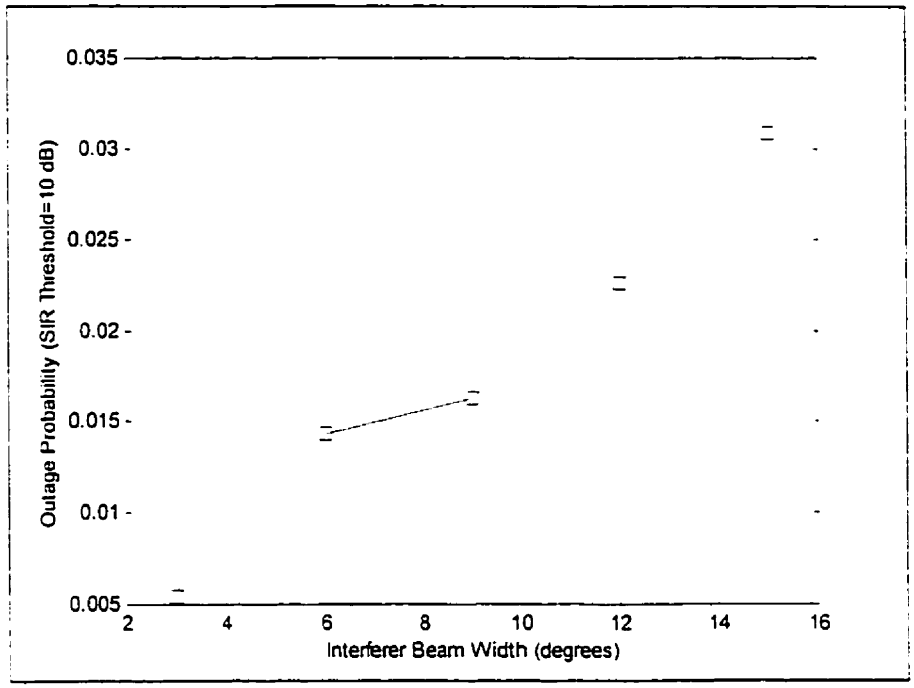

P= 30 dBw, BSBW= 120°, BSGR=30 dB, INTGR=30 dB, n=4, σ=14 dB

Figure 5.10 Effect of Interferer Antenna Beam Width

The outage probability increased from 0.5% at 3° beam width to 3.1% at 15°.

Figure 5.11 shows the similar result when the base station antennas beam widths are increased from 20° to 140°. An increase in outage probability is evident with larger base station beam widths. This indicates that the expense of dividing a base station into sectors will be rewarded by lower outage probability. A steady rise in interference level is expected since each base station is more likely to apply the higher gain to the interfering signal with increased beam width.

The outage probability increased from nearly no outage at 20° beam width, to 1.3% at 140° beam width.

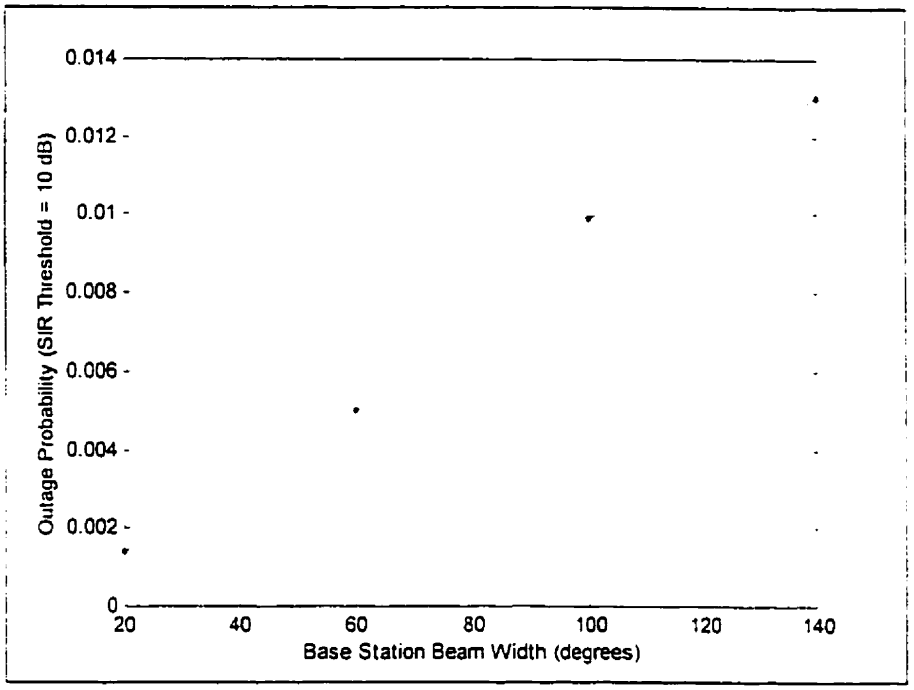

P= 30 dBw, INTBW= 5°, BSGR=30 dB, INTGR=30 dB, n=4, σ=14 dB

Figure 5.11 Effect of Base Station Antenna Beam Width

5.2.3.2 Effect of Antenna Gain Ratios

The results of increasing the antenna gain ratio of both the interferer and base station antennas are shown in Figures 5.12 and 5.13, respectively. Both show a linear decrease in the outage probability as the gain ratio is increased.

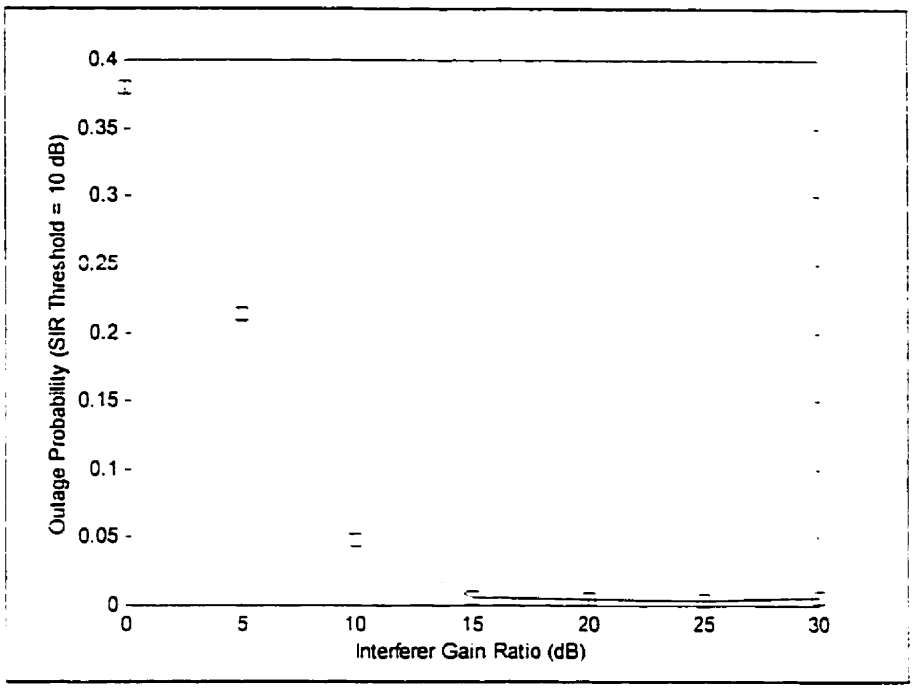

P= 30 dBw, BSBW= 120°, INTBW= 5°, BSGR=30 dB, n=4, σ=14 dB

Figure 5.12 Effect of Interferer Gain Ratio

The outage probability decreases much more rapidly with increased interferer gain ratio than it does for the base station. Indeed, the probability of outage decreased from 38% at an interferer gain ratio 0 dB to approximately 0.5% at an gain ratio of 30 dB whereas the outage probability only experienced a 1.7% drop for the same increase in base station gain ratio. The difference is that after a gain ratio of 15 dB, any further increase in interferer gain ratio had no effect. However, after the same point, increasing the base station gain ratio further increased the outage probability, albeit slightly. This serves to highlight the sensitivity of system performance to subscriber and base station antenna gains.

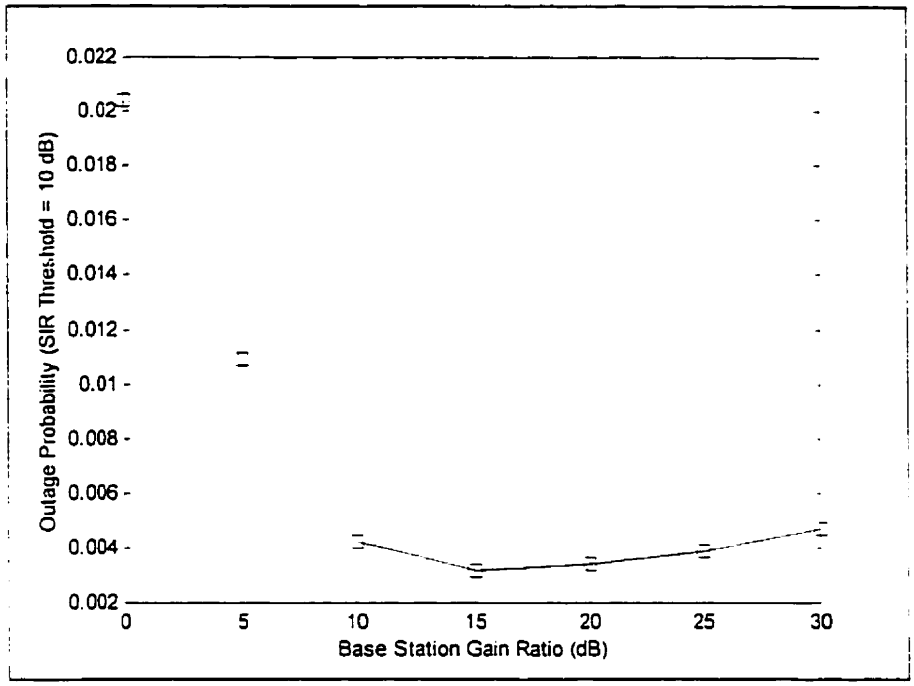

P= 30 dBw, BSBW= 120°, INTBW= 5°, INTGR=30 dB n=4, σ=14 dB

Figure 5.13 Effect of Base Station Gain Ratio

5.2.3.3 Effect of Realistic Base Station Antenna Pattern

Figure 5.14 illustrates the difference in interference levels when a realistic antenna beam pattern is used compared with the ideal (two-valued) beam pattern used up until this point.

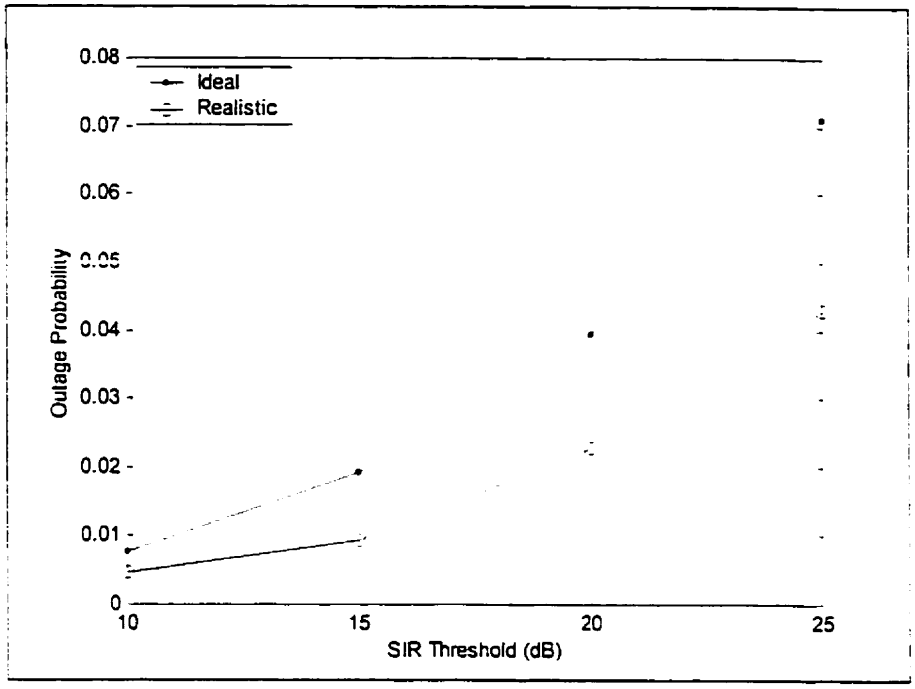

P= 30 dBw, BSBW= 120°, INTBW= 5°, BSGR=30 dB, INTGR=30 dB, n=4, σ=14 dB

Figure 5.14 Effect of Realistic Base Station Antenna Beam Patterns

The outage probabilities obtained with the realistic base station antenna pattern are consistently lower than those of the ideal antenna pattern. At a SIR threshold of 10 dB, the difference between the model antenna pattern and the realistic antenna pattern was slight (0.3%) whereas at a threshold of 25 dB, the difference was 2.8%. However, as both the curves closely follow each other, the ideal antenna pattern is judged to be a valid simplification for simulation proposes, particularly when a SIR threshold of 10 dB was predominately used.

5.2.5 Effect of Hub Sector Size

When the cells of the model are divided into sectors, the simulation yields results shown in Figure 5.15.

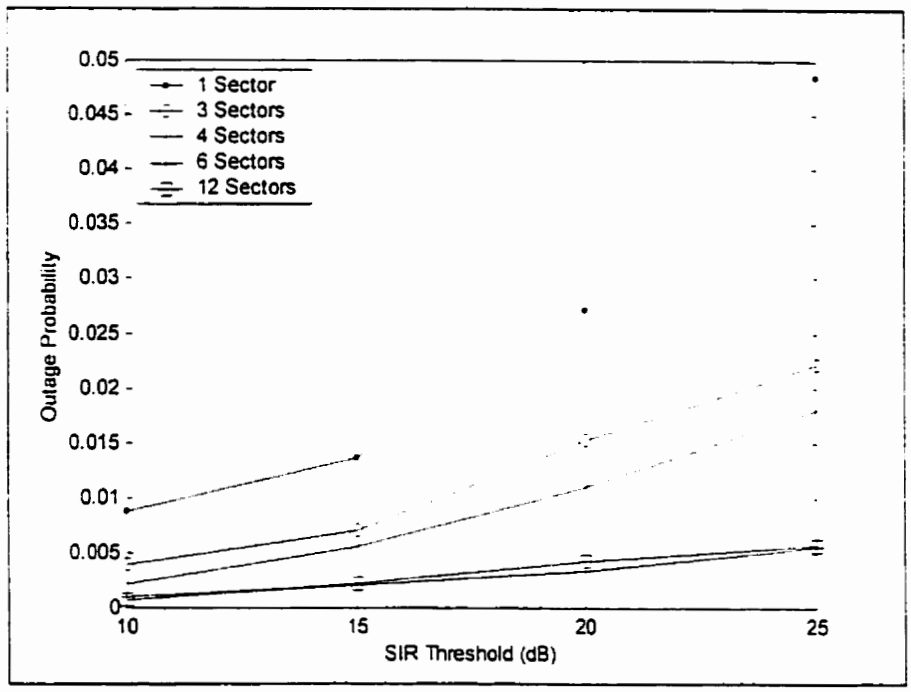

P= 30 dBw, INTBW= 5°, BSGR=30 dB, INTGR=30 dB, n=4, σ=14 dB

Figure 5.15 Effect of Hub Sector Size

The lowest outage occurred with the 12-sector system although nearly the same outage probability occurred with a 6-sector system. Note the diminishing returns of sectorization: with each increase in sector size, the corresponding outage benefit is smaller. For example, at a SIR threshold of 20 dB, the outage decreased 1.2% when going from an omni-directional system (1-sector) to a 3-sector system. Another 0.4% drop was experienced moving to a 4-sector system, then a 0.8% drop occurred when moving to a 6-sector system. There was only a slight difference between the 6-sector

system and the 12-sectors system. After some point, the considerable infrastructure expense of sectorization will not be economical for the performance enhancement it will provide. Still, some degree of sectorization is deemed beneficial.

5.2.5 Effect of Base Station Diversity

As expected, Figure 5.16 shows that the outage probability decreases when base station diversity is used for several SIR thresholds.

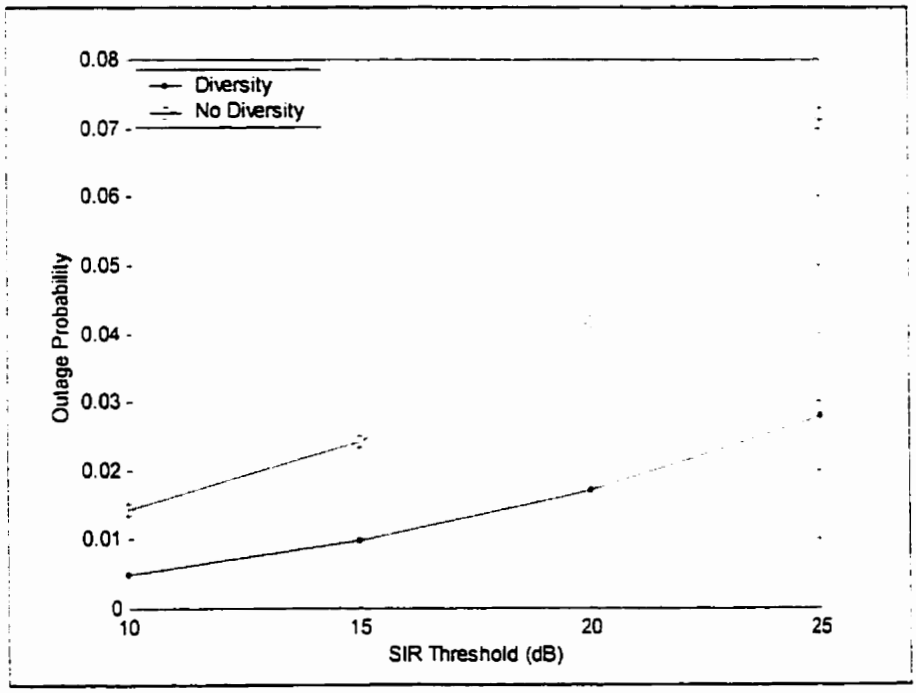

P= 30 dBw, BSBW= 120°, INTBW= 5°, BSGR=30 dB, INTGR=30 dB, n=4, σ=14 dB

Figure 5.16 Effect of Base Station Diversity

Relaxing the diversity condition produced a dramatic system performance gain. Indeed, at a SIR threshold of 15 dB, the outage probability was only 1.0% for a system with base station diversity as compared to an outage probability of 2.4% for a system with no diversity. The effect increased at larger SIR thresholds indicating that base

station diversity results in a higher average SIR and therefore yields a lower outage probability. Other investigations have yielded similar results [11].

This shows that providing the subscriber the ability to home in on the base station that has the lowest path loss associated with it will significantly enhance system performance. This is due to the fact that when subscribers home in on the base station with the least path loss, they will use the least transmitter power and thus will be contributing the least amount of interference to the cellular network.

5.3 Model Comparison

This section compares the results produced by the two different methods of simulation: the simplified version that has been used in section 5.2, and the full version which includes 100 subscribers. Figure 5.17 shows that the results from the simulation with one subscriber are very similar to those produced by a corresponding simulation with 100 subscribers (one in every cell). Thus, the simplified model introduced in section 5.1.2 is found to be equivalent to the general approach and is a valid method of reducing the number of calculations required by the simulation.

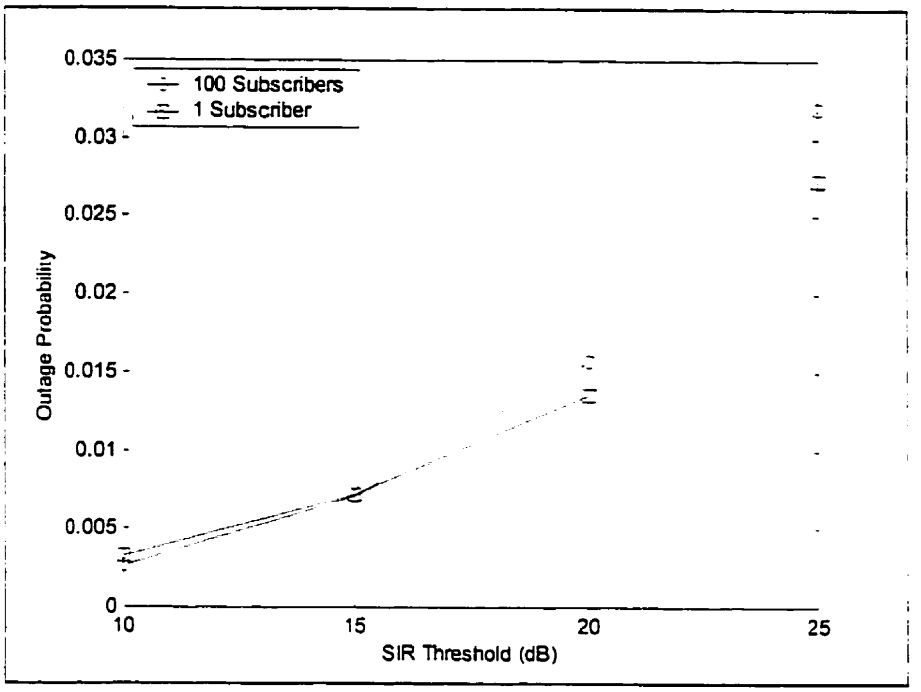

P= 30 dBw, BSBW= 120°, INTBW= 5°, BSGR=30 dB, INTGR=30 dB n=4, σ=10 dB

Figure 5.17 Model Comparison

5.4 Goodness of Fit to Normal Distribution

The Kolmogorov-Smirnov Test [36, 37] is employed to test the distribution of interference to determine how closely it follows a Gaussian distribution. The Kolmogorov-Smirnov goodness of fit test measures the degree of agreement between distributions of a sample of empirically gathered values and a target distribution. The Kolmogorov-Smirnov statistic is defined by [37]:

$$D_n = \max[|F_n(x) - F_o(x)|] \qquad \text{over all } x \tag{5.18}$$

where: $F_n(x)$ is the empirical function being tested, and

$F_o(x)$ is the hypothesized function for the random variable X.

The hypothesis that $F_n(x) = F_o(x)$ is rejected if D_n is too large, which is determined by comparing the computed D_n with published critical values [37]. In this case, a logarithmic scale is needed to evaluate the interference statistics, which are also on a logarithmic scale. Thus, the $F_o(x)$ used is [30,31]:

$$F_o(x) = 1 - \frac{1}{2} erfc\left(\frac{x-\mu}{2\sigma}\right) \tag{5.19}$$

where: μ , σ are the mean and standard deviation on a logarithmic scale.

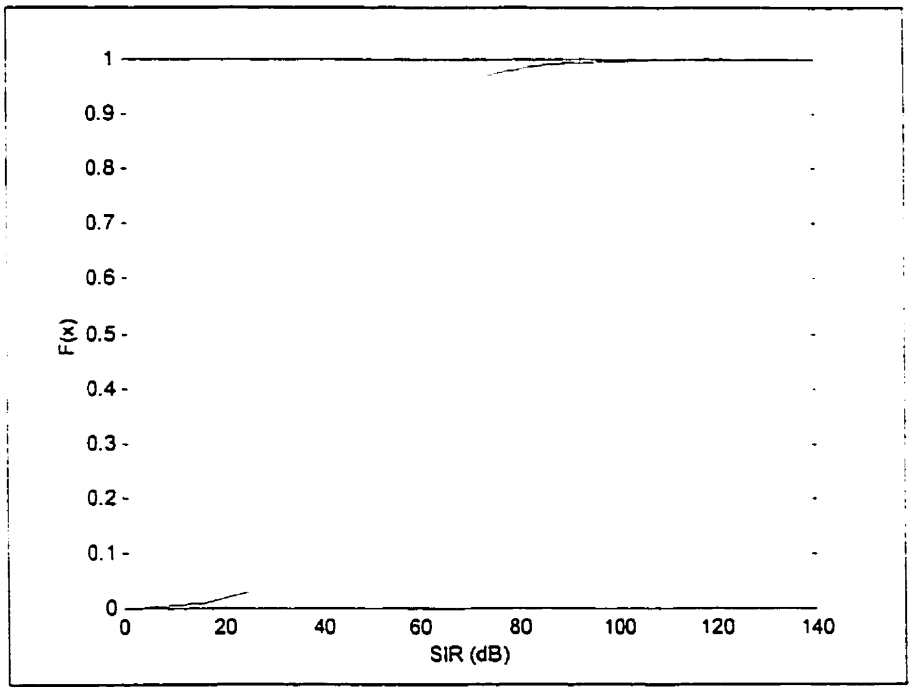

P= 30 dBw, BSBW= 120°, INTBW= 5°, BSGR=30 dB, INTGR=30 dB n=4, σ=14 dB

Figure 5.18 SIR Cumulative Distribution Function

The distribution of SIR is tested with the Kolmogrov-Smirnov test with the significance level of 0.1. The computed statistic, 0.08435 is smaller than the critical value, 0.136. Thus, the cumulative distribution of interference power shown in Figure

5.18 does not significantly differ from that of a Gaussian distribution and the distribution of interference powers is deemed to closely follow a log-normal distribution.

5.5 Discussion

The interference contributed to the base stations furthest from the subscriber was found to be minimal. Thus, a further simplification could be made by computing only the interference a single subscriber contributes to its nearest neighbours. This would vastly reduce the number of calculations required, but would still be a valid simulation since the cells immediately surrounding the subscriber experience a preponderance of the interference.

As discussed previously, thermal noise was not included in this simulation. Therefore, only outage probability due to interference is reported here, not coverage. As found in the measurements, there are holes in the coverage where no discernable signal energy could be detected. Thus, actual outage probabilities will be greater than those reported in this work.

Since the subscriber's location was chosen randomly in the simulated LMCS network, the outage probability calculations could be slightly biased by the edge effect. That is, when the subscriber's location is chosen close to the edge of the network, the total interference it contributes will be less than that contributed by a subscriber which is completely surrounded by base stations. Therefore, slightly higher outage probabilities

could be expected if one compensated for the edge effect by only picking subscriber locations in the interior of the network.

5.6 Summary of results

The simulation evaluated the effect of several parameters on the outage probabilities encountered in a simplified interference model of a LMCS network.

The probability of outage was found to decrease from 1.6% to 0.3% as the propagation exponent increased from 2 to 5. An increase of 1% in outage was found when the standard deviation of log-normal shadowing was varied from 0 to 20 dB. Both the subscriber and base station antenna beam widths were found to linearly increase the outage probability as they were increased. Modification of the gain ratio of both the subscriber and base station antennas was found to correspond to a direct decrease in outage probability. A change in interferer gain ratio from 0 to 30 dB caused the greatest outage decrease of 38%. A realistic antenna beam pattern was found to yield a performance enhancement in a range of 0.3% to 2.8% for different SIR thresholds when compared to the model antenna beam pattern. Sectorization lowered the outage probability with the largest effect at lower sector sizes. Finally, relaxing the base station diversity condition showed that diversity yields a performance gain with as much as a 2.4% decrease in outage probability.

The single subscriber model was compared with the general model with 100 subscribers. The performance of both models was found to be equivalent.

The distribution of interference powers was not found to significantly differ from a log-normal distribution when tested with the Kolmogrov-Smirnov test on a logarithmic scale at a significance level of 0.1.

Chapter Six

CONCLUSIONS AND RECOMMENDATIONS

6.1 Conclusions

A propagation measurement campaign was conducted followed by modelling and simulation to predict the interference contributed to a LMCS network by a single subscriber. The object was to evaluate the LMCS radio channel in a NLOS environment.

Field measurements show that propagation at 29.5 GHz in a developed urban environment will attenuate with a propagation exponent of 4.01 for NLOS locations with measurements in the noise removed. A 13.89 dB degree of shadowing was observed. No significant signal energy was detected in off bore-sight angles likely due to the narrow beam width of the antenna.

The simulation evaluated the effect of several parameters on the outage probabilities encountered in a simplified interference model of a LMCS network. Both the propagation exponent and the degree of shadowing affected the probability of outage. A high propagation exponent attenuated interference resulting in a lower outage probability.

It was found that system performance is highly sensitive to the subscriber and hub antenna gain ratios, and beam widths. Lower outage can be obtained through the use of highly directional subscriber antennas with large gains.

Sectorization lowered the outage probability with the largest effect at lower sector sizes. Relaxing the base station diversity condition showed that diversity yields a performance gain with a decrease in outage probability at all SIR thresholds.

The single subscriber model was compared with the general model with 100 subscribers. The performance of both models was found to be equivalent.

The distribution of interference powers was not found to significantly differ from a log-normal distribution when tested with the Kolmogrov-Smirnov test on a logarithmic scale at a significance level of 0.1.

The major contribution of this thesis is to identify the interference that can be expected at the base station of a cell in a LMCS network. Propagation measurements are used to produce a more statistically significant simulation of the interference in a LMCS network. The observed path loss exponent along with the standard deviation of log-normal shadowing are found to be consistent with previously reported results.

A simplified interference model reveals the limitations on system performance that interference in a LMCS system imposes. A high propagation exponent is demonstrated to reduce the outage probability by attenuating signal levels. Antenna design and sectoring is shown to affect LMCS performance by lowering interference levels. Further, simulated base station diversity has been shown to reduce the interference experienced at the base station and is an important component of LMCS design.

6.2 Recommendations for Future Research

Ground level measurements were less difficult to carry out than roof level measurements would have been. However, roof level measurements may provide a more accurate description of the LMCS radio channel as the subscriber antennas will be fixed on or near the roof of residential buildings.

There has been some research to suggest that use of specular reflections would enhance coverage of LMCS networks. Although no significant signal energy was found in off bore-sight angles, further investigation is warranted. The narrow beam width of the antennas along with the fact that the measurements sites were NLOS and at ground level, likely limited our ability to detect energy at off bore-sight angles.

The measurements were taken in August and early September 1999. The trees in the Glebe were in full foliage and would have provided the maximum signal attenuation of the year. As such, the measurements reported in this work represent a worst-case propagation scenario. However, measurements at different times during the year would reveal the expected difference in signal levels and will indicate the degree of increased coverage that can be expected when the foliage is less than that of summer.

A parameter of propagation at EHF frequencies that has not been significantly researched is that of the standard deviation of the log-normal shadowing and whether or not it varies with T-R distance. This work did not cover enough measurement sites to determine conclusively whether or not the variance changes with distance.

The simulation did not include Rayleigh fading which may significantly contribute to propagation mechanisms in a LMCS system. However, its effects would likely be less than in a comparable mobile cellular system.

REFERENCES

[1] Industry Canada, Local Multipoint Communications Systems (LMCS) in the 28 GHz Range: Policy, Authorization Procedures and Evaluation Criteria, 1996.

[2] G.M. Stamatelos, and D.D. Falconer, "Millimeter Radio Access to Multimedia Services via LMDS," *Proceedings of Globecom*, London, November 1996.

[3] W. Honcharenko, J.P. Kruys, D.Y. Lee, and N.J. Shah, "Broadband Wireless Access," *IEEE Communications Magazine*, January 1997, pp. 20-26.

[4] K.C. Chua, K.V. Ravi, B. Bensaou, and T.C. Pek, "Wireless Broadband Communications: Some Research Activities in Singapore," *IEEE Communications Magazine*, November 1999, pp. 84-90.

[5] N. Naz, "Temporal Variation Characterization for LMCS Channel and System Design Implications," M.Eng Thesis, Department of Systems and Computer Engineering, Carleton University, March 1999. Also: N. Naz and D.D. Falconer, "Temporal Variations Characterization for Fixed Wireless at 29.5 GHz," Proceedings of VTC 2000, Tokyo, May 2000.

[6] L.M. Correia and R.Prasad, "An Overview of Wireless Broadband Communications," *IEEE Communications Magazine*, January 1997, pp. 28-33.

[7] Industry Canada: strategis.ic.gc.ca

[8] Canadian Wireless Telecommunications Association: www.cwta.ca

[9] IEEE Broadband Wireless Access Standards Working Group (802.16): www.ieee802.org/16/coexistence/

[10] P.B. Papazian, G.A. Hufford, R.J. Achatz, and R. Hoffman, "Study of the Local Mulitipoint Distribution Service Radio Channel," *IEEE Transactions on Broadcasting*, Vol. 43, No. 2, June 1997

[11] J.P. DeCruyenaere and D.D. Falconer, "Propagation Simulation for the Prediction of LMCS/LMDS Coverage," Presented at ANTEM'98, Ottawa, August 1998.

[12] E.J. Violette, R.H. Espeland, R. and F. Schwering, "Millimeter-Wave Propagation at Street Level in and Urban Environment," *IEEE Transactions on Geoscience and Remote Sensing*, Vol. 26, No. 3, 1988.

[13] S.Y. Seidel and H.W. Arnold, "Propagation Measurements at 28 GHz to Investigate the Performance of Local Multipoint Distribution Service (LMDS)," Proceedings of Globecom. Singapore, November 1995. pp. 754-757.

[14] F.K. Schwering, E.J. Violette, and R.H. Espeland, "Millimeter-Wave Propagation in Vegetation: Experiments and Theory," *IEEE Transactions on Geoscience and Remote Sensing*, Vol. 26, No. 3, May 1988, pp. 355-367.

[15] Theodore S. Rappaport, *Wireless Communications, Principles and Practice*. Prentice Hall PTR, 1996.

[16] P. Newson and M.R. Heath, "The Capacity of a Spread Spectrum CDMA System for Cellular Mobile Radio with Consideration of System Imperfections," *IEEE Journal on Selected Areas in Communications*, Vol. 12, No. 4, May 1994, pp. 673-683.

[17] K.S. Gilhousen, I.M. Jacobs, R. Padovani, A.J. Viterbi, L.A. Weaver Jr. and C.E. Wheatley III, "On the Capacity of a Cellular CDMA System," *IEEE Transactions on Vehicular Technology*, Vol. 40, No. 2, May 1991, pp. 303-312.

[18] N.C. Beaulieu, A.A. Abu-Dayya, and P.J. McLane, "Estimating the Distribution of a Sum of Independent Lognormal Random Variables," *IEEE Transactions on Communications*, Vol. 43, No. 12, December 1995, pp. 2869-2873.

[19] Y.S. Yeh, and S.C. Schwartz, "Outage Probability in Mobile Telephony Due to Multiple Log-Normal Interferers," *IEEE Transactions on Communications*, Vol. Com-32, No. 4, April 1984, pp. 380-388.

[20] W.A. Janos, "Tail of the Distribution of Sums of Log-Normal Variates," *IEEE Transactions on Information Theory*, Vol. IT-16, No. 3, May 1970, pp. 299-302.

[21] A. Safak, "Statistical Analysis of the Power Sum of Multiple Correlated Log-Normal Components," *IEEE Transactions on Vehicular Technology*, Vol. 42, No. 1, February 1993, pp.58-63.

[22] S.C. Schwartz, and Y.S. Yeh, "On the Distribution Function and Moments of Power Sums with Log-Normal Components," *Bell System Technical Journal*, Vol. 61, No. 7, September 1982, pp. 1441-1462.

[23] JP.M.G. Linnartz, "Exact Analysis of the Outage Probability in Multiple-User Mobile Radio," *IEEE Transactions on Communications*, Vol. 40, No. 1, January 1992, pp. 20-23.

[24] A.A. Abu-Dayya, and N.C. Beaulieu, "Outage Probabilities in the Presence of Correlated Lognormal Interferers," *IEEE Transactions on Vehicular Technology*, Vol. 43, No. 1, February 1994, pp 164-172.

[25] M. Zorzi, "On the Analytical Computation of the Interference Statistics with Applications to the Performance Evaluation of Mobile Radio Systems," *IEEE Transactions on Communications*, Vol. 45, No. 1, January 1997, pp. 103-109.

[26] D. C. Cox, "Universal Digital Portable Radio Communications", *Proceedings of the IEEE*, Vol.75, No. 4, April 1987, pp. 436-477.

[27] D.O. Reudink, "Properties of Mobile Radio Propagation Above 400 MHz," *IEEE Transactions on Vehicular Technology*, Vol. VT-23, No. 4, November 1974, pp. 143-159.

[28] V.K. Garg, and J.E. Wilkes, *Wireless and Personal Communication Systems*. Prentice Hall PTR, 1996.

[29] S.Y. Seidel, T.S. Rappaport, S. Jain, M.L. Lord and R. Singh, "Path Loss, Scattering, and Multipath Delay Statistics in Four European Cities for Digital Cellular and Microcellular Radiotelephone," *IEEE Transactions on Vehicular Technology*, Vol. 40, 1991, pp. 721-730.

[30] S.Q. Gong, "Outage Performance with Directional Antennas in Cellular Fixed Broadband Access Systems," M.Eng Thesis, Department of Systems and Computer Engineering, Carleton University, January 1997.

[31] S.Q. Gong and D.D. Falconer, "Cochannel Interference in Cellular Fixed Broadband Access Systems with Directional Antennas," *Wireless Personal Communications*, Vol. 10, 1998, pp. 103-117.

[32] D.C. Cox, "Cochannel Interference Considerations In Frequency Reuse Small-Coverage-Area Radio Systems," *IEEE Transactions on Communications*, Vol. Com-30, No. 1, 1982, pp. 135-142.